

# Towards Lightweight Super-Resolution with Dual Regression Learning

Yong Guo, Jingdong Wang, Qi Chen, Jiezhong Cao, Zeshuai Deng, Yanwu Xu, Jian Chen, Mingkui Tan\*

**Abstract**—Deep neural networks have exhibited remarkable performance in image super-resolution (SR) tasks by learning a mapping from low-resolution (LR) images to high-resolution (HR) images. However, the SR problem is typically an ill-posed problem and existing methods would come with several limitations. First, the possible mapping space of SR can be extremely large since there may exist many different HR images that can be downsampled to the same LR image. As a result, it is hard to directly learn a promising SR mapping from such a large space. Second, it is often inevitable to develop very large models with extremely high computational cost to yield promising SR performance. In practice, one can use model compression techniques to obtain compact models by reducing model redundancy. Nevertheless, it is hard for existing model compression methods to accurately identify the redundant components due to the extremely large SR mapping space. To alleviate the first challenge, we propose a dual regression learning scheme to reduce the space of possible SR mappings. Specifically, in addition to the mapping from LR to HR images, we learn an additional dual regression mapping to estimate the downsampling kernel and reconstruct LR images. In this way, the dual mapping acts as a constraint to reduce the space of possible mappings. To address the second challenge, we propose a lightweight dual regression compression method to reduce model redundancy in both layer-level and channel-level based on channel pruning. Specifically, we first develop a channel number search method that minimizes the dual regression loss to determine the redundancy of each layer. Given the searched channel numbers, we further exploit the dual regression manner to evaluate the importance of channels and prune the redundant ones. Extensive experiments show the effectiveness of our method in obtaining accurate and efficient SR models.

**Index Terms**—Image Super-Resolution; Dual Regression; Closed-loop Learning; Lightweight Models.

## 1 INTRODUCTION

DEEP neural networks (DNNs) have been the workhorse of many real-world applications, including image classification [1], [2] and image restoration [3], [4], [5], [6], [7], [8], [9], [10], [11], [12], [13], [14]. Recently, image super-resolution (SR) has become an important task that aims to learn a non-linear mapping to reconstruct high-resolution (HR) images from low-resolution (LR) images. Nevertheless, the SR problem is typically an ill-posed problem and it is non-trivial to learn an effective SR model due to several underlying challenges.

First, the space of possible SR mapping functions can be extremely large since there exist many HR images that can be downsampled to the same LR image [15]. As a result, it is hard to directly learn a good solution from a large mapping space. To alleviate this issue, existing methods seek to increase the model capacity (*e.g.*, EDSR [16] and RCAN [17]) and minimize the reconstruction error between the super-resolved images and the ground-truth HR images. However, these methods still suffer from such a large space of possible SR mapping functions (See more analysis in Section 3.1) and often yield limited performance. Thus, how to reduce the possible space of the mapping functions to boost the training of SR models becomes an important problem.

Second, most SR models often contain a large number of parameters and come with extremely high computational cost. To address this, many efforts have been made to design efficient SR models [18], [19]. However, these models often incur a dramatic performance gap compared with state-of-the-art SR methods [20], [21]. Unlike these methods, one can also exploit model compression techniques (*e.g.*, channel pruning) to obtain lightweight models. Nevertheless, it is non-trivial to identify the redundant components (*e.g.*, channels) in SR models due to the large possible mapping space. Specifically, given an inaccurate SR mapping, the estimated/predicted redundancy of model components may be also very inaccurate. More critically, the redundancy may vary a lot among different layers in the model and different channels in each layer, making it harder to identify the redundant components.

In this paper, we propose a novel dual regression learning scheme to obtain accurate and efficient SR models. To reduce the possible mapping space, we introduce an additional constraint that encourages the super-resolved images to reconstruct the input LR images. Ideally, if the mapping LR→HR is optimal, the super-resolved images can be easily downsampled to obtain the original input LR image. With this constraint, the dual regression scheme improves SR performance by reducing the space of possible SR mappings and yielding a smaller generalization bound than existing methods (See Theorem 1). To obtain effective lightweight SR models, we propose a lightweight dual regression compression method to reduce the model redundancy in both layer-level and channel-level. Specifically, we first determine the redundancy of each layer by performing channel number search. Then, we exploit the dual regression scheme to evaluate the importance of channels and prune those redundant ones according to the searched channel numbers. Extensive experiments demonstrate the superiority of our method (See results in Fig. 4).

- Yong Guo, Zeshuai Deng, Jian Chen, and Mingkui Tan are with the School of Software Engineering, South China University of Technology. Yong Guo is also with the Max Planck Institute for Informatics. E-mail: guoyongcs@gmail.com, sedengzeshuai@mail.scut.edu.cn, {ellachen, mingkui-tan}@scut.edu.cn
- Jingdong Wang is with the Microsoft Research Asia. E-mail: jingdw@microsoft.com
- Qi Chen is with the Faculty of Engineering, the University of Adelaide. E-mail: qi.chen04@adelaide.edu.au
- Jiezhong Cao is with ETH Zürich. E-mail: jiezhong.cao@vision.ee.ethz.ch
- Yanwu Xu is with the Baidu Inc. E-mail: ywxu@ieee.org
- \* Corresponding author.

Our contributions are summarized as follows:

- To alleviate the issue of extremely large SR mapping space incurred by the nature of ill-posed problems, we propose a dual regression learning scheme that introduces an additional dual mapping to reconstruct LR images. The dual mapping acts as a constraint to reduce the space of possible SR mapping functions and enhance the training of SR models.
- Unlike existing model compression methods, we propose a lightweight dual regression compression method that exploits a reduced mapping space to identify both the layer-level and channel-level redundancy. Specifically, we first perform channel number search to determine the redundancy of each layer by minimizing the dual regression loss. With the searched channel numbers, we further exploit the dual regression manner to evaluate the importance of channels for channel pruning.
- Extensive experiments on several benchmark datasets demonstrate the efficacy of our method in obtaining effective lightweight SR models. In practice, our lightweight dual regression compression method greatly reduces the computational cost (in terms of both model size and inference latency) without significant performance drop.

This paper extends our preliminary version [22] from several aspects. 1) We propose a lightweight dual regression compression scheme to obtain effective lightweight SR models. 2) We present a dual regression based channel number search method to identify the layer-level redundancy by determining the number of channels for each layer. 3) We develop a dual regression based channel pruning algorithm that exploits the dual regression manner to evaluate the importance of channels when performing channel pruning. 4) We conduct more ablation studies to investigate the effect of the proposed channel number search method and channel pruning method. 5) We compare the inference speed of different SR models on CPU devices to demonstrate the effectiveness of our method in obtaining lightweight models.

## 2 RELATED WORK

### 2.1 Image Super-resolution

Existing SR methods mainly includes interpolation-based approaches [23], [24], [25], [26] and reconstruction-based methods [17], [27], [28], [29], [30]. Interpolation-based methods may oversimplify the SR problem and usually generate blurry images [31], [32]. The reconstruction-based methods [33], [34], [35] reconstruct the HR images from LR images. Following such methods, many CNN-based methods [36], [37], [38], [39], [40], [41], [42] were developed to learn a reconstruction mapping.

Recently, Ledig *et al.* [31] propose a deep residual network SRResNet for super-resolution. Lim *et al.* [16] remove unnecessary modules in the residual network [1] and design a very wide network EDSR. Haris *et al.* [27] propose a back-projection network (DBPN) to iteratively produce LR and HR images. Zhang *et al.* [17] propose a channel attention mechanism to build a deep model called RCAN to further improve the SR performance. Mei *et al.* [20] propose a Cross-Scale Non-Local attention module for more accurate image SR. Niu *et al.* [21] propose a holistic attention network (HAN) to model the interdependencies among layers, channels, and spatial positions. Liang *et al.* [43] develop a transformer model to improve the performance of image restoration. However, the training process of these methods still has a very large space of the possible SR mappings, making it hard to learn a good solution in practice.

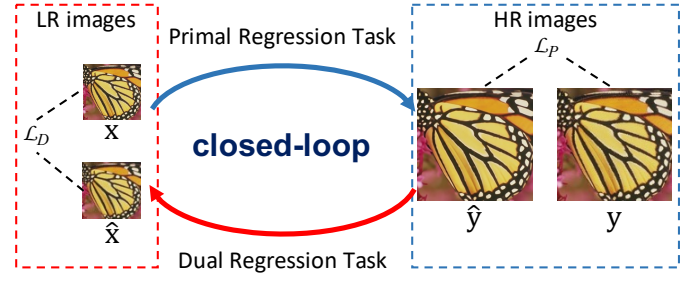


Fig. 1. The proposed dual regression learning scheme contains a primal regression task for SR and a dual regression task to reconstruct LR images. The primal and dual regression tasks form a closed-loop.

### 2.2 Lightweight Model Techniques

Lightweight models have gained great attention in recent years. One can obtain lightweight models by directly designing efficient architectures or distilling knowledge from other models. Hui *et al.* [19] propose an information distillation block to extract the local long and short-path features for lightweight SR networks. Zhang *et al.* [44] propose a re-parameterizable building block for efficient SR. However, these models often incur a dramatic performance gap compared to state-of-the-art SR methods [20], [21]. Besides these methods, one can enhance the lightweight SR performance using knowledge distillation technique [45], [46], [47]. Gao *et al.* [45] use a lightweight student SR model to learn the knowledge from the deeper teacher SR network. Lee *et al.* [46] propose a distillation framework that leverages HR images as privileged information to boost the training of the student network.

Besides these methods, we can also use model compression techniques to obtain lightweight models [48], [49], [50], [51]. As one of the predominant approaches, channel pruning [52], [53], [54], [55], [56], [57] seeks to remove the redundant channels of deep models to obtain compact subnets. It has been shown that these subnets often come with promising accuracy [58] and robustness [59], [60], [61]. Recently, Li *et al.* [62] propose a differentiable meta channel pruning method (DHP) to compress SR models. In additional, some quantization-based methods [63], [64], [65] exploit low bits to accelerate the inference speed of SR models. However, it is still non-trivial for these methods to identify the redundant components due to the extremely large possible function space. Unlike them, we seek to reduce the possible function space to alleviate the training/compression difficulty. Thus, it becomes possible to obtain lightweight SR models without significant performance degradation (See Fig. 4).

### 2.3 Dual Learning

Dual learning [66], [67], [68], [69] contains a primal model and a dual model and learns two opposite mappings simultaneously to enhance the performance of language translation. Recently, this scheme has also been used to perform image translation without paired training data [70], [71]. Specifically, a cycle consistency loss is proposed to avoid the mode collapse issue of GAN methods [70], [72], [73] and help minimize the distribution divergence. However, these methods cannot be directly applied to the standard SR problem. By contrast, we use the closed-loop to reduce the space of possible functions of SR. Moreover, we consider learning asymmetric mappings and provide a theoretical guarantee on the rationality and necessity of using a cycle.

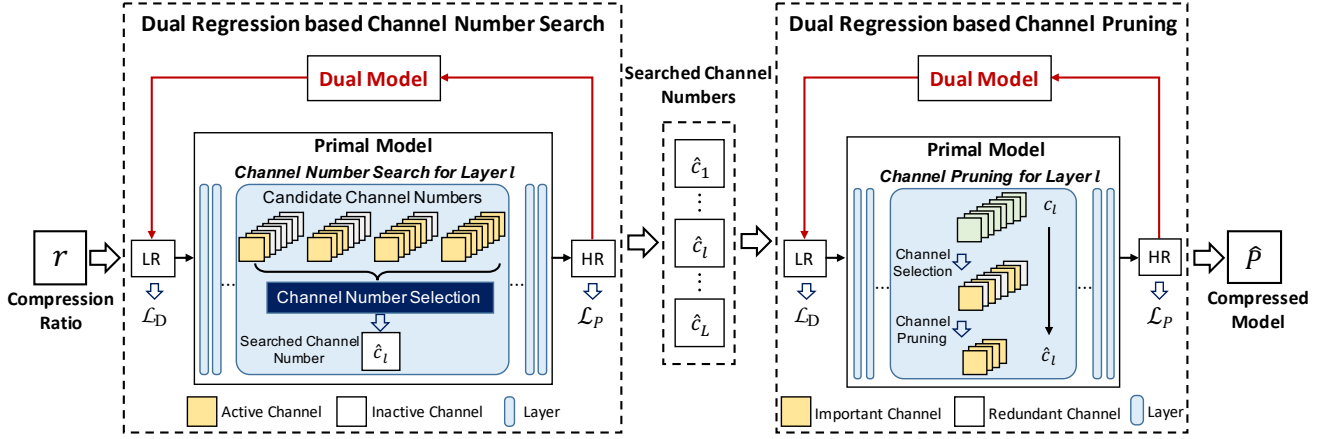


Fig. 2. Overview of the lightweight dual regression compression approach. Given a target compression ratio  $r$ , we first determine the redundancy of each layer by performing the dual regression based channel number search. Then, according to the searched channel numbers, we evaluate the importance of channels and prune those redundant ones to obtain the compressed model  $\hat{P}$ .

### 3 DUAL REGRESSION NETWORKS

In this paper, we propose a dual regression learning scheme to obtain accurate and efficient SR models. As shown in Fig. 1, we introduce a constraint on LR images to reduce the space of possible SR mapping functions. To further reduce the model redundancy, we propose a lightweight dual regression compression method to compress large models (See Fig 2). For convenience, we term our models Dual Regression Networks (DRNs).

#### 3.1 Dual Regression Learning for Super-Resolution

Due to the nature of the ill-posed problems, the space of possible SR mapping functions can be extremely large, making the training very difficult. To alleviate this issue, we propose a dual regression learning scheme by introducing an additional constraint on LR data. From Fig. 1, besides the mapping  $LR \rightarrow HR$ , we also learn an inverse/dual mapping from the super-resolved images back to LR images. Let  $\mathbf{x} \in \mathcal{X}$  be LR images and  $\mathbf{y} \in \mathcal{Y}$  be HR images. Unlike existing methods, we simultaneously learn a primal mapping  $P$  to reconstruct HR images and a dual mapping  $D$  to reconstruct LR images. Formally, we formulate the SR problem into the dual regression learning scheme which involves two regression tasks.

**Definition 1 (Primal Regression Task for SR)** We seek to find a function  $P: \mathcal{X} \rightarrow \mathcal{Y}$ , such that the prediction  $P(\mathbf{x})$  is similar to its corresponding HR image  $\mathbf{y}$ .

**Definition 2 (Dual Regression Task for SR)** We seek to find a function  $D: \mathcal{Y} \rightarrow \mathcal{X}$ , such that the prediction of  $D(\mathbf{y})$  is similar to the original input LR image  $\mathbf{x}$ .

The primal and dual learning tasks form a closed-loop and provide important supervision to train the models  $P$  and  $D$ . If  $P(\mathbf{x})$  was the correct HR image, then the downsampled image  $D(P(\mathbf{x}))$  should be very close to the input LR image  $\mathbf{x}$ . By jointly learning these two tasks, we train the models based on  $N$  paired samples  $\{(\mathbf{x}_i, \mathbf{y}_i)\}_{i=1}^N$ , where  $\mathbf{x}_i$  and  $\mathbf{y}_i$  denote the  $i$ -th pair of LR and HR images. Let  $\mathcal{L}_P$  and  $\mathcal{L}_D$  be the loss function ( $\ell_1$ -norm) for

the primal and dual tasks, respectively. The training loss becomes

$$\mathcal{L}_{DR}(P, D) = \underbrace{\frac{1}{N} \sum_{i=1}^N \mathcal{L}_P(P(\mathbf{x}_i), \mathbf{y}_i)}_{\text{primal regression loss}} + \underbrace{\lambda \mathcal{L}_D(D(P(\mathbf{x}_i)), \mathbf{x}_i)}_{\text{dual regression loss}}. \quad (1)$$

Here,  $\lambda$  controls the weight of the dual regression loss (See the sensitivity analysis of  $\lambda$  in Section 5.4).

More critically, we also theoretically justify our method. In practice, our method has a smaller generalization bound than the vanilla training methods (*i.e.*, without the dual mapping). In other words, our method helps to learn a more accurate  $LR \rightarrow HR$  mapping and improve SR performance. We summarize the theoretical analysis in Theorem 1 and put the proof in supplementary.

**Theorem 1** Let  $\mathcal{L}_{DR}(P, D)$  be a mapping from  $\mathcal{X} \times \mathcal{Y}$  to  $[0, 1]$  and  $\mathcal{H}_{dual}$  be the function space. Let  $N$  denote the number of samples and  $\hat{R}_{\mathcal{Z}}^{DL}$  represent the empirical Rademacher complexity [74] of dual learning. We use  $\mathcal{B}(P), P \in \mathcal{H}$  to denote the generalization bound of the supervised learning w.r.t. the Rademacher complexity  $\hat{R}_{\mathcal{Z}}^{SL}(\mathcal{H})$ . For any error  $\delta > 0$ , the generalization bound of the dual regression scheme is  $\mathcal{B}(P, D) = 2\hat{R}_{\mathcal{Z}}^{DL}(\mathcal{H}_{dual}) + 3\sqrt{\frac{1}{2N} \log(\frac{2}{\delta})}$ . Based on the definition of the Rademacher complexity, the capacity of the function space  $\mathcal{H}_{dual}$  is smaller than the capacity of function space  $\mathcal{H}$ , *i.e.*,  $\hat{R}_{\mathcal{Z}}^{DL} \leq \hat{R}_{\mathcal{Z}}^{SL}$ . In this sense, the dual regression scheme has a smaller generalization bound than the vanilla learning scheme:

$$\mathcal{B}(P, D) \leq \mathcal{B}(P).$$

**Differences from CycleGAN based methods [70], [71].** Both DRN and CycleGAN [70] exploit the similar idea of building a cycle, but they have several essential differences. First, they consider different objectives. CycleGAN uses cycles to help minimize distribution divergence but DRN builds a cycle to improve reconstruction performance. Second, they consider different cycle/dual mappings. CycleGAN learns two symmetric mappings but DRN considers learning asymmetric mappings. Essentially, the primal mapping  $LR \rightarrow HR$  is much more complex than the dual mapping  $HR \rightarrow LR$ . Considering this, we design the dual model with a very small CNN (See the detailed model design in supplementary) and introduce a tradeoff parameter  $\lambda$  in Eqn. (1).

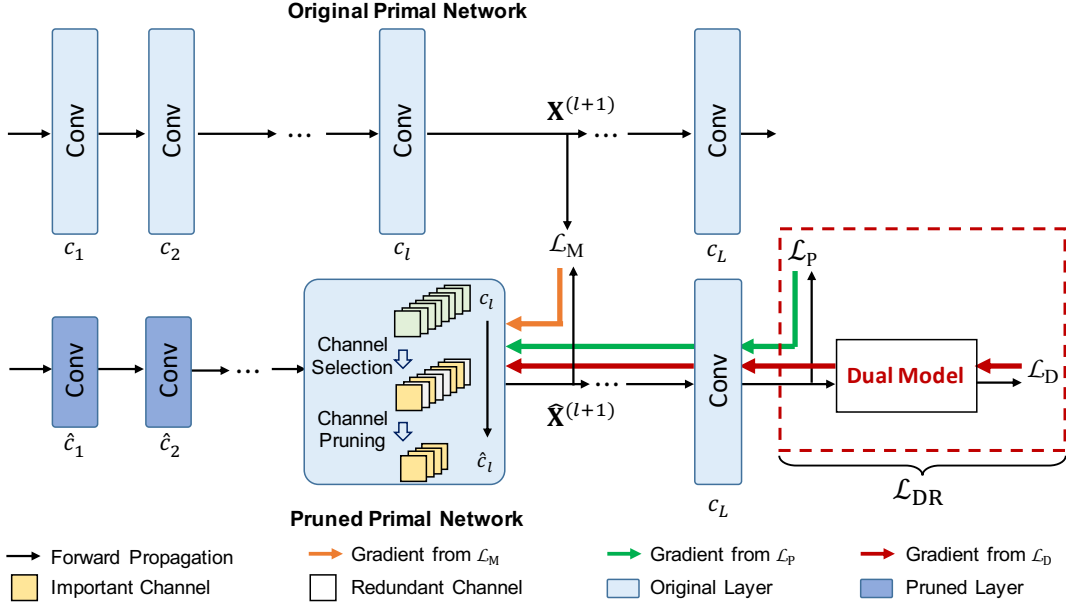


Fig. 3. The dual regression based channel pruning method. We evaluate the importance of channels by computing both the feature reconstruction loss  $\mathcal{L}_M$  and the dual regression loss  $\mathcal{L}_{DR}$ . Here,  $\mathbf{X}^{(l+1)}$  and  $\hat{\mathbf{X}}^{(l+1)}$  denote the output features of the  $l$ -th layer in the original model and the pruned model, respectively.  $c_l$  and  $\hat{c}_l$  denote the channel number of the  $l$ -th layer in the original model and the pruned model.

---

**Algorithm 1:** Dual Regression based Channel Number Search

---

**Input:** Training data  $\mathcal{S}^{\text{train}}$  and validation data  $\mathcal{S}^{\text{val}}$ ;  
Original channel numbers  $\{c_l\}_{l=1}^L$ ;  
Channel number configurations  $\{\alpha_l\}_{l=1}^L$ ;  
Candidate scaling factors  $\mathcal{V}$ ;  
Target compression ratio  $r$ .

**Output:** Searched channel numbers  $\{\hat{c}_l\}_{l=1}^L$ .

```

1 Rebuild model  $\alpha$  with configuration parameters  $\{\alpha_l\}_{l=1}^L$ ;
2 while not converge do
3   // Update the channel number configuration  $\alpha$ 
4   Sample data batch from  $\mathcal{S}^{\text{val}}$  to compute  $\mathcal{L}_{DR}^{\text{val}}$ ;
5   Update  $\alpha$  by descending  $\nabla_{\alpha} \mathcal{L}_{DR}^{\text{val}}((\alpha; \mathbf{W}^*), D)$ 
6   // Update model parameters  $\mathbf{W}$ 
7   Sample data batch from  $\mathcal{S}^{\text{train}}$  to compute  $\mathcal{L}_{DR}^{\text{train}}$ ;
8   Update  $\mathbf{W}$  by descending  $\nabla_{\mathbf{W}} \mathcal{L}_{DR}^{\text{train}}((\alpha; \mathbf{W}), D)$ 
9 end
10 for  $l = 1$  to  $L$  do
11   Select the scaling factor  $\hat{v} = \arg \max_{v \in \mathcal{V}} \alpha_l^{(v)}$ ;
12   Compute the channel number  $\hat{c}_l = c_l \cdot (1 - r) \cdot \hat{v}$ ;
13 end
```

---

### 3.2 Lightweight Dual Regression with Channel Pruning

Most SR models have extremely high computational cost and cannot be directly deployed to the devices with limited computation resources. To alleviate this issue, one can apply model compression techniques to obtain lightweight models. However, it is non-trivial to accurately identify the redundant components (e.g., layers or channels) due to the extremely mapping space. Specifically, once we learn an inaccurate SR mapping, the predicted model redundancy may be also inaccurate, leading to significant performance drop (See results in Table 3).

To address the above issues, we build a lightweight dual regression compression method based on channel pruning tech-

niques to compress SR models in a reduced mapping space. Let  $\psi(\cdot)$  be the function to measure the computational cost of models (e.g., the number of parameters). Given a primal model  $P$  and a target compression ratio  $r$ , we seek to obtain a compressed model  $\hat{P}$  that satisfies the constraint  $\psi(\hat{P}) \leq (1 - r)\psi(P)$ . Supposing that both  $P$  and  $\hat{P}$  share the same dual model  $D$ , the optimization problem becomes:

$$\min_{\hat{P}} \mathcal{L}_{DR}(\hat{P}, D) \quad \text{s.t.} \quad \psi(\hat{P}) \leq (1 - r)\psi(P). \quad (2)$$

In this paper, we seek to reduce the model redundancy in both layer-level and channel-level. As shown in Fig. 2, we first determine the redundancy for each layer by performing dual regression channel number search. Then, we exploit the dual regression scheme to evaluate the importance of channels and prune the redundant ones according to the searched channel numbers.

#### 3.2.1 Dual Regression based Channel Number Search

Most channel pruning methods adopt a hand-crafted compression policy to prune deep models [75], [76], e.g., pruning 50% channels in all the layers. However, such a compression policy may not be optimal since different layers often have different redundancy [77]. To address this issue, we propose a dual regression channel number search method to recognize the redundancy of each layer by determining the promising number of channels to be preserved. We show the details of the proposed method in Algorithm 1.

Given a primal model  $P$  with  $L$  layers, we use  $\{c_l\}_{l=1}^L$  to denote the channel numbers of different layers. To obtain a model that satisfies the target compression ratio  $r$ , for any layer  $l$ , we first remove  $c_l \cdot r$  channels and then investigate whether we can further remove more channels without degrading the performance. Nevertheless, the search space would be extremely large since the candidate channel number can be any positive integer lower than  $c_l$ . To alleviate this issue, we construct the search space by considering a set of candidate scaling factors  $\mathcal{V} = \{50\%, 60\%, 70\%, 80\%, 90\%, 100\%\}$  to scale the channel



number. Specifically, for the  $l$ -th layer, we seek to select a scaling factor  $\hat{v} \in \mathcal{V}$  to obtain the resultant channel number  $\hat{c}_l = c_l \cdot (1 - r) \cdot \hat{v}$  in the compressed model.

To find the promising channel numbers, we adopt the differentiable search strategy [78] by relaxing the search space to be continuous. For any layer  $l$ , we construct a channel number configuration  $\alpha_l \in \mathbb{R}^{|\mathcal{V}|}$  in which each element  $\alpha_l^{(v)}$  indicates the importance of a specific scaling factor  $v$ . For any layer  $l$ , let  $\mathbf{X}^{(l)}$  be the input features,  $\mathbf{W}^{(l)}$  be the parameters, and  $\otimes$  be the convolutional operation. For convenience, we use  $\mathbf{X}_{[1:k]}^{(l)}$  and  $\mathbf{W}_{[1:k]}^{(l)}$  to denote the features and parameters *w.r.t.* the first  $k$  channels. In this paper, we use  $c_l^{(v)}$  to denote the number of channels specified by a specific scaling factor  $v$ . Following [78], we relax the categorical choice of a particular factor as a softmax over all possible factors. Formally, the output of the  $l$ -th layer is

$$\mathbf{X}^{(l+1)} = \sum_{v \in \mathcal{V}} \frac{\exp(\alpha_l^{(v)})}{\sum_{v' \in \mathcal{V}} \exp(\alpha_l^{(v')})} \mathbf{X}_{[1:c_l^{(v)}]}^{(l)} \otimes \mathbf{W}_{[1:c_l^{(v)}]}^{(l)}. \quad (3)$$

With the continuous relaxation, the task of channel number search becomes learning a set of continuous variables  $\alpha = \{\alpha_l\}_{l=1}^L$ . As shown in Algorithm 1, for any layer  $l$ , we obtain the resultant channel numbers by selecting the most likely element in  $\alpha_l$ .

To enhance the search process, we minimize the dual regression loss to reduce the space of possible mapping functions. Let  $\mathcal{L}_{\text{DR}}^{\text{train}}$  and  $\mathcal{L}_{\text{DR}}^{\text{val}}$  be the dual regression loss computed on the training data and validation data. Here, we use the continuous variables  $\alpha$  and the model parameters  $\mathbf{W}$  to represent the primal model  $P = (\alpha; \mathbf{W})$ . Given a dual model  $D$ , the optimization problem of channel number search becomes

$$\begin{aligned} \min_{\alpha} \quad & \mathcal{L}_{\text{DR}}^{\text{val}}((\alpha; \mathbf{W}^*), D) \\ \text{s.t.} \quad & \mathbf{W}^* = \arg \min_{\mathbf{W}} \mathcal{L}_{\text{DR}}^{\text{train}}((\alpha; \mathbf{W}), D). \end{aligned} \quad (4)$$

### 3.2.2 Dual Regression based Channel Pruning

Based on the searched channel numbers, we still need to determine which channels should be pruned. One of the key challenges is how to accurately evaluate the importance of channels. To address this, we develop a dual regression channel pruning method that exploits the dual regression scheme to identify the important channels. We show our method in Fig. 3.

Let  $P$  and  $\hat{P}$  be the original primal model and the compressed model, respectively. We use  $\mathbf{X}^{(l+1)}$  and  $\hat{\mathbf{X}}^{(l+1)}$  to denote the output feature maps of the  $l$ -th layer in  $P$  and  $\hat{P}$ . Given the searched channel numbers  $\{\hat{c}_l\}_{l=1}^L$ , we seek to select the channels which really contribute to SR performance. Nevertheless, this goal is non-trivial to achieve due to the extremely large mapping space incurred by the ill-posed problem. To address this issue, we exploit the dual regression scheme to evaluate the importance of channels. Specifically, we consider one channel as an important one if it helps to reduce the dual regression loss  $\mathcal{L}_{\text{DR}}(\hat{P}, D)$ . Moreover, for any layer  $l$ , we also minimize the reconstruction error [75], [79] of the feature maps between  $P$  and  $\hat{P}$ , *i.e.*,  $\mathcal{L}_{\text{M}}(\mathbf{X}^{(l+1)}, \hat{\mathbf{X}}^{(l+1)})$ , to further improve the performance. Given a specific channel number  $\hat{c}_l$ , we impose an  $\ell_0$ -norm constraint  $\|\mathbf{W}^{(l)}\|_0 \leq \hat{c}_l$  on the number of active channels in  $\mathbf{W}^{(l)}$ . Formally, the channel pruning problem for the  $l$ -th layer is:

$$\min_{\mathbf{W}^{(l)}} \mathcal{L}_{\text{M}}(\mathbf{X}^{(l+1)}, \hat{\mathbf{X}}^{(l+1)}) + \gamma \mathcal{L}_{\text{DR}}(\hat{P}, D), \quad \text{s.t.} \quad \|\mathbf{W}^{(l)}\|_0 \leq \hat{c}_l, \quad (5)$$

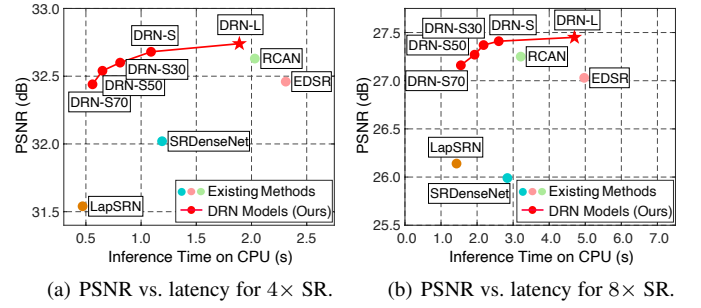


Fig. 4. Comparisons of the performance (in terms of PSNR) and the inference latency (on the Intel Core i5-8500 CPU) of different models for 4 $\times$  and 8 $\times$  SR on the Set5 dataset.

where  $\gamma$  is a hyper-parameter that controls the weight of the dual regression loss (See more discussions on  $\gamma$  in Section 5.5). However, Problem (5) is hard to solve due to the training difficulty incurred by the  $\ell_0$ -norm constraint. To address this, we adopt a greedy strategy [52], [80], [81] in which we first remove all the channels and then select the most important channels one by one. Following [52], we perform channel selection according to the gradients *w.r.t.* different channels.

## 4 EXPERIMENTS

We conduct extensive experiments to verify the effectiveness of the proposed methods. First, we evaluate the proposed dual regression learning scheme for 4 $\times$  and 8 $\times$  SR. Then, we compare the proposed dual regression compression method with existing model compression methods. The source code is available at <https://github.com/guoyongcs/DRN>.

### 4.1 Datasets and Implementation Details

Based on the dual regression scheme, we build our DRN based on the design of U-Net for SR [91], [92] (See more details in the supplementary materials). We first propose two models, including a small model DRN-S and a large model DRN-L. Then, we use the proposed dual regression compression method to compress the DRN-S model. We consider three compression ratios  $\{30\%, 50\%, 70\%\}$  to obtain three lightweight SR models, namely DRN-S30, DRN-S50, and DRN-S70.

**Datasets and evaluation metrics.** Following [90], we train our models on DIV2K [93] and Flickr2K [16] datasets, which contain 800 and 2650 images separately. For quantitative comparison, we evaluate different SR methods on five benchmark datasets, including Set5 [94], Set14 [95], BSDS100 [96], Urban100 [97] and Manga109 [98]. To assess the quality of super-resolved images, we adopt two commonly used metrics, *i.e.*, PSNR and SSIM [99]. The computational cost #MAdds and the latency on Intel Core i5-8500 CPU are measured on a  $96 \times 96$  LR image.

**Training details.** During training, we apply Adam [100] with  $\beta_1 = 0.9$ ,  $\beta_2 = 0.99$  and set minibatch size as 32. We use RGB input patches with size  $48 \times 48$  from LR images and the corresponding HR patches as the training data, and augment the training data following the method in [16], [17]. The learning rate is initialized to  $10^{-4}$  and decreased to  $10^{-7}$  with a cosine annealing out of  $10^6$  iterations. As for the model compression, we obtain the compressed lightweight model from the pre-trained DRN-S model and finetune its parameters.

TABLE 1  
Performance comparisons with state-of-the-art methods for  $4\times$  image super-resolution. “-” denotes the results that are not reported.

Method	#Params (M)	#MAdds (G)	CPU Latency (s)	Set5 PSNR / SSIM	Set14 PSNR / SSIM	BSDS100 PSNR / SSIM	Urban100 PSNR / SSIM	Manga109 PSNR / SSIM
Bicubic	—	—	—	28.42 / 0.810	26.10 / 0.702	25.96 / 0.667	23.15 / 0.657	24.92 / 0.789
SRCNN [82]	0.1	8.5	0.09	30.48 / 0.863	27.49 / 0.750	26.90 / 0.710	24.52 / 0.722	27.66 / 0.851
FSRCNN [18]	—	0.7	—	30.71 / 0.866	27.59 / 0.754	26.98 / 0.710	24.62 / 0.728	27.90 / 0.852
ESPCN [83]	—	0.2	—	29.21 / 0.851	26.40 / 0.744	25.50 / 0.696	24.02 / 0.726	23.55 / 0.795
LapSRN [84]	0.9	29.2	0.47	31.54 / 0.885	28.09 / 0.770	27.31 / 0.727	25.21 / 0.756	29.09 / 0.890
DRRN [85]	0.3	1087.5	0.44	31.68 / 0.889	28.21 / 0.772	27.38 / 0.728	25.44 / 0.764	29.46 / 0.896
CARN [86]	1.1	14.6	0.44	32.13 / 0.894	28.60 / 0.781	27.58 / 0.735	26.07 / 0.784	30.47 / 0.908
CARN-M [86]	0.3	5.2	11.80	31.92 / 0.890	28.42 / 0.776	27.44 / 0.730	25.62 / 0.769	25.62 / 0.769
IMDN [87]	0.7	6.6	0.25	32.21 / 0.895	28.58 / 0.781	27.56 / 0.735	26.04 / 0.784	30.45 / 0.908
PAN [88]	0.3	4.5	0.18	32.13 / 0.895	28.61 / 0.782	27.59 / 0.736	26.11 / 0.785	30.51 / 0.910
SRResNet [31]	1.5	20.5	0.17	32.05 / 0.891	28.49 / 0.782	27.61 / 0.736	26.09 / 0.783	30.70 / 0.908
SRGAN [31]	1.5	20.5	0.12	29.46 / 0.838	26.60 / 0.718	25.74 / 0.666	24.50 / 0.736	27.79 / 0.856
SRDenseNet [32]	2.0	62.3	1.19	32.02 / 0.893	28.50 / 0.778	27.53 / 0.733	26.05 / 0.781	29.49 / 0.899
EDSR [16]	43.1	463.3	2.31	32.48 / 0.898	28.81 / 0.787	27.72 / 0.742	26.64 / 0.803	31.03 / 0.915
DBPN [27]	15.3	1220.4	5.72	32.42 / 0.897	28.75 / 0.786	27.67 / 0.739	26.38 / 0.794	30.90 / 0.913
RCAN [17]	15.6	147.1	2.03	32.63 / 0.900	28.85 / 0.788	27.74 / 0.743	26.74 / 0.806	31.19 / 0.917
SAN [89]	15.8	150.1	16.58	32.64 / 0.900	28.92 / 0.788	27.79 / 0.743	26.79 / 0.806	31.18 / 0.916
RRDB [90]	16.7	165.5	2.14	32.73 / 0.901	28.97 / 0.790	27.83 / 0.745	27.02 / 0.815	31.64 / 0.919
CSNLTN [20]	6.6	4428.5	—	32.68 / 0.900	28.95 / 0.789	27.80 / 0.744	<b>27.22 / 0.817</b>	31.43 / 0.920
HAN [21]	16.2	151.5	1.76	32.61 / 0.900	28.90 / 0.789	27.79 / 0.744	26.85 / 0.809	31.44 / 0.918
ECBSR [44]	0.6	5.5	0.09	31.92 / 0.895	28.34 / 0.782	27.48 / 0.739	25.81 / 0.777	—
DRN-S70	1.4	32.8	0.56	32.39 / 0.897	28.74 / 0.785	27.67 / 0.739	26.43 / 0.795	30.94 / 0.914
DRN-S50	2.3	53.1	0.65	32.47 / 0.898	28.85 / 0.788	27.72 / 0.741	26.62 / 0.802	31.22 / 0.916
DRN-S30	3.1	72.3	0.81	32.60 / 0.899	28.89 / 0.788	27.76 / 0.742	26.76 / 0.805	31.36 / 0.917
DRN-S	4.8	109.9	1.09	32.68 / 0.901	28.93 / 0.790	27.78 / 0.744	26.84 / 0.807	31.52 / 0.919
DRN-L	9.8	224.8	1.89	<b>32.74 / 0.902</b>	<b>28.98 / 0.792</b>	<b>27.83 / 0.745</b>	27.03 / 0.813	<b>31.73 / 0.922</b>

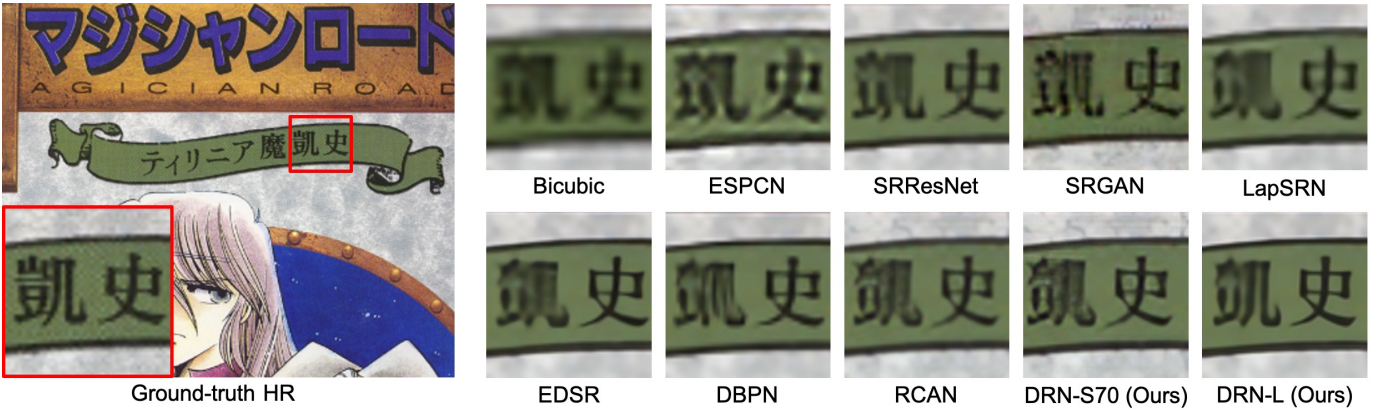


Fig. 5. Visual comparisons of the images produced by different models for  $4\times$  image super-resolution on benchmark datasets.

#### Details of channel number search and channel pruning.

We search the channel numbers in each layer for the compressed models on DIV2K [93] dataset. Following [78], we use zero initialization for the continuous variables  $\alpha$ , which ensures  $\alpha$  to receive sufficient learning signal at the early stage. We use Adam [100] optimizer to train the model with the learning rate  $\eta = 3 \times 10^{-4}$  and the momentum  $\beta = (0.9, 0.999)$ . We train the channel number search model for 100 epochs with the batch size of 16. The channel number search process takes approximately 3 hours on a TITAN Xp GPU. As for channel pruning, we perform dual regression channel pruning to select important channels on DIV2K [93] dataset. During pruning, once we remove the input channels of the  $l$ -th convolution layer, the output channels of the previous convolution layer can be removed correspondingly. Once a new channel is selected, to reduce the performance drop, we apply the SGD optimizer with a learning rate of  $5 \times 10^{-5}$  to update the parameters of selected channels for one epoch.

#### 4.2 Comparisons with State-of-the-art SR Methods

In this experiment, we compare our method with state-of-the-art SR methods in terms of both quantitative results and visual results. For the quantitative comparison, we show the PSNR and SSIM values of different methods for  $4\times$  and  $8\times$  super-resolution in Table 1 and Table 2. Then, for quality comparison, we provide visual comparisons for our method and the considered methods in Fig. 5 and Fig. 6. Last, we compare the latency of our models with state-of-the-art methods and show the results in Fig. 4.

From Table 1 and Table 2, our large model DRN-L achieves the best results on most benchmark datasets. When we decrease the number of channels and layers, our small baseline model DRN-S also obtains promising performance. After compression, our compressed DRN models still yield promising performance. For example, our smallest DRN-S70 model yields a comparable performance with the large EDSR and DBPN models. From Fig. 5 and Fig. 6, our model consistently produces sharper edges and

TABLE 2  
Performance comparisons with state-of-the-art algorithms for  $8\times$  image super-resolution. “-” denotes the results that are not reported.

Algorithm	#Params (M)	#MAdds (G)	CPU Latency (s)	Set5 PSNR / SSIM	Set14 PSNR / SSIM	BSDS100 PSNR / SSIM	Urban100 PSNR / SSIM	Manga109 PSNR / SSIM
Bicubic	—	—	—	24.39 / 0.657	23.19 / 0.568	23.67 / 0.547	20.74 / 0.515	21.47 / 0.649
SRCNN [82]	0.1	33.8	0.48	25.33 / 0.689	23.85 / 0.593	24.13 / 0.565	21.29 / 0.543	22.37 / 0.682
FSRCNN [18]	—	2.8	0.06	25.41 / 0.682	23.93 / 0.592	24.21 / 0.567	21.32 / 0.537	22.39 / 0.672
ESPCN [83]	—	0.4	0.03	25.02 / 0.697	23.45 / 0.598	23.92 / 0.574	21.20 / 0.554	22.04 / 0.683
LapSRN [84]	0.8	93.9	1.43	26.14 / 0.737	24.35 / 0.620	24.54 / 0.585	21.81 / 0.580	23.39 / 0.734
DRRN [85]	0.3	4350.2	—	25.76 / 0.721	24.21 / 0.583	24.47 / 0.533	21.02 / 0.530	21.88 / 0.663
SRResNet [31]	1.7	49.2	1.14	26.62 / 0.756	24.55 / 0.624	24.65 / 0.587	22.05 / 0.589	23.88 / 0.748
SRGAN [31]	1.7	49.2	1.14	23.04 / 0.626	21.57 / 0.495	21.78 / 0.442	19.64 / 0.468	20.42 / 0.625
SRDenseNet [32]	3.3	471.8	2.84	25.99 / 0.704	24.23 / 0.581	24.45 / 0.530	21.67 / 0.562	23.09 / 0.712
EDSR [16]	45.5	814.4	4.97	27.03 / 0.774	25.05 / 0.641	24.80 / 0.595	22.55 / 0.618	24.54 / 0.775
DBPN [27]	34.0	10360.9	22.30	27.25 / 0.786	25.14 / 0.649	24.90 / 0.602	22.72 / 0.631	25.14 / 0.798
RCAN [17]	15.7	169.6	3.21	27.31 / 0.787	25.23 / 0.651	24.96 / 0.605	22.97 / 0.643	25.23 / 0.802
SAN [89]	16.0	172.6	17.66	27.22 / 0.782	25.14 / 0.647	24.88 / 0.601	22.70 / 0.631	24.85 / 0.790
HAN [21]	16.2	174.1	—	27.29 / 0.788	25.23 / 0.651	24.96 / 0.605	22.98 / 0.644	25.20 / 0.801
DRN-S70	1.6	53.6	1.55	27.16 / 0.783	25.13 / 0.646	24.91 / 0.601	22.76 / 0.631	25.07 / 0.796
DRN-S50	2.5	94.5	1.93	27.26 / 0.785	25.14 / 0.648	24.94 / 0.602	22.78 / 0.633	25.13 / 0.799
DRN-S30	3.5	124.1	2.18	27.37 / 0.790	25.25 / 0.651	24.97 / 0.604	22.94 / 0.640	25.29 / 0.804
DRN-S	5.4	197.9	2.60	27.41 / 0.790	25.25 / 0.652	24.98 / 0.605	22.96 / 0.641	25.30 / 0.805
DRN-L	10.0	366.5	4.70	<b>27.43 / 0.792</b>	<b>25.28 / 0.653</b>	<b>25.00 / 0.606</b>	<b>22.99 / 0.644</b>	<b>25.33 / 0.806</b>

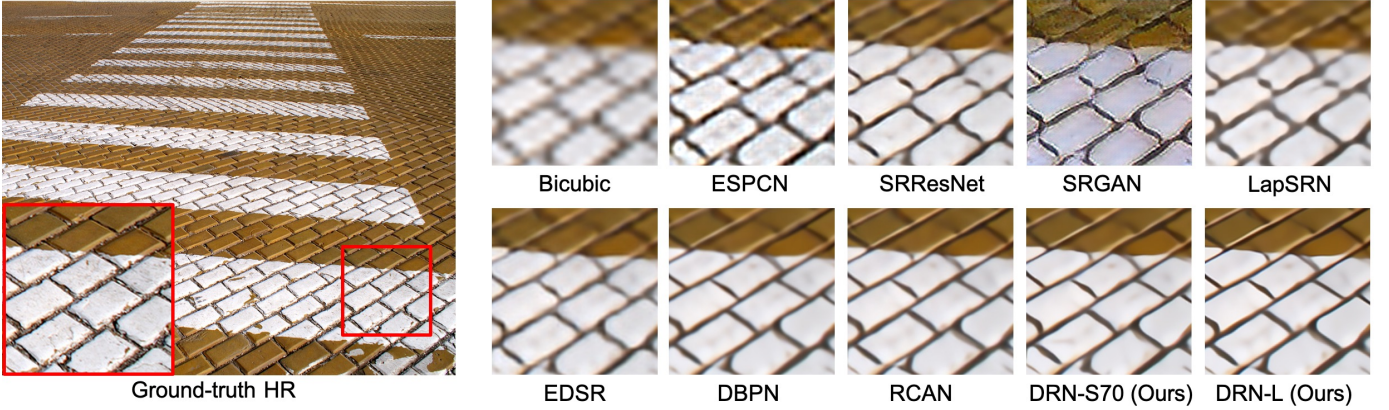


Fig. 6. Visual comparisons of the images produced by different models for  $8\times$  image super-resolution on benchmark datasets.

shapes for both  $4\times$  and  $8\times$  SR, while other baselines may produce blurrier ones (See more results in the supplementary materials).

Moreover, we compare the inference latency of our DRN models with others on CPU devices for  $4\times$  and  $8\times$  SR. From Fig. 4, our DRN-S obtains promising performance with small latency. When we further compressed our DRN-S models, our compressed DRN models are more efficient on model inference. Both the empirical results and the theoretical analysis in Theorem 1 show the effectiveness of our dual regression learning scheme for accurate and efficient super-resolution networks.

### 4.3 Comparisons with Model Pruning Methods

To demonstrate the effectiveness of our compression method, we compare our lightweight dual regression compression method and several existing channel pruning methods, including CP [101], Thinet [50], and DCP [52]. We apply the considered methods to compress the DRN-S model for  $4\times$  and  $8\times$  SR. From Table 3, given the same compression ratio, the compressed SR models obtained by our proposed dual regression compression method consistently outperform those models obtained by the other methods. Moreover, our compressed models consistently have less computational cost in the same target compression ratio.

The experiment demonstrates the effectiveness of our proposed lightweight dual regression compression method (See more discussions in Section 5.2 and Section 5.3).

## 5 FURTHER EXPERIMENTS

In this section, we provide more discussions on the dual regression learning scheme. First, we conduct ablation studies on the dual regression learning scheme in Section 5.1. Second, we verify the effect of the dual regression channel number search method in Section 5.2. Third, we investigate the effect of the dual regression pruning method in Section 5.3. Then, we analyze the effect of the hyper-parameter  $\lambda$  and  $\gamma$  in Sections 5.4 and 5.5, respectively. Last, we further investigate the effect of an additional cycle constraint on the HR domain in Section 5.6.

### 5.1 Effect of Dual Regression Learning Scheme

We conduct an ablation study on our dual regression learning scheme and report the results for  $4\times$  SR in Table 4. We evaluate the dual regression learning scheme on both our DRN-S and DRN-L models and show the experimental results on five benchmark datasets. From Table 4, compared to the baselines, the models



TABLE 3

Performance comparisons of the pruned models obtained by different channel pruning methods on  $4\times$  and  $8\times$  SR. We adopt DRN-S as the baseline model and the MAdds is calculated on a  $96 \times 96$  LR image.

Scale	Compression Ratio	Method	#Params (M)	#MAdds (G)	Set5 PSNR / SSIM	Set14 PSNR / SSIM	BSDS100 PSNR / SSIM	Urban100 PSNR / SSIM	Manga109 PSNR / SSIM
4	0%	Baseline	4.8	109.9	32.68 / 0.901	28.93 / 0.790	27.78 / 0.744	26.84 / 0.807	31.52 / 0.919
	30%	CP [101]	3.4	77.4	32.26 / 0.887	28.47 / 0.777	27.38 / 0.732	26.42 / 0.794	31.03 / 0.904
		Thinet [50]			32.33 / 0.889	28.57 / 0.781	27.45 / 0.734	26.53 / 0.796	31.12 / 0.907
		DCP [52]			32.41 / 0.893	28.65 / 0.782	27.52 / 0.737	26.61 / 0.800	31.21 / 0.912
		DRN-S30			<b>32.60 / 0.899</b>	<b>28.89 / 0.788</b>	<b>27.76 / 0.742</b>	<b>26.76 / 0.805</b>	<b>31.36 / 0.917</b>
	50%	CP [101]	2.4	55.2	32.17 / 0.885	28.41 / 0.775	27.35 / 0.732	26.38 / 0.793	30.73 / 0.901
		Thinet [50]			32.26 / 0.888	28.55 / 0.780	27.42 / 0.734	26.49 / 0.796	30.81 / 0.904
		DCP [52]			32.34 / 0.891	28.62 / 0.782	27.49 / 0.737	26.53 / 0.798	30.95 / 0.909
		DRN-S50			<b>32.47 / 0.898</b>	<b>28.85 / 0.788</b>	<b>27.72 / 0.741</b>	<b>26.62 / 0.802</b>	<b>31.22 / 0.916</b>
	70%	CP [101]	1.5	34.6	32.05 / 0.882	28.34 / 0.772	27.33 / 0.729	26.12 / 0.785	30.57 / 0.903
		Thinet [50]			32.16 / 0.886	28.51 / 0.778	27.47 / 0.731	26.25 / 0.789	30.70 / 0.906
		DCP [52]			32.27 / 0.890	28.63 / 0.781	27.61 / 0.734	26.32 / 0.792	30.84 / 0.911
		DRN-S70			<b>32.39 / 0.897</b>	<b>28.74 / 0.785</b>	<b>27.67 / 0.739</b>	<b>26.43 / 0.795</b>	<b>30.94 / 0.914</b>
8	0%	Baseline	5.4	198.0	27.41 / 0.790	25.25 / 0.652	24.98 / 0.605	22.96 / 0.641	25.30 / 0.805
	30%	CP [101]	3.8	140.8	27.14 / 0.782	25.07 / 0.645	24.74 / 0.598	22.74 / 0.635	25.09 / 0.797
		Thinet [50]			27.26 / 0.786	25.14 / 0.648	24.85 / 0.601	22.84 / 0.638	25.18 / 0.801
		DCP [52]			27.30 / 0.787	25.17 / 0.649	<b>24.97 / 0.604</b>	22.90 / 0.639	25.25 / 0.803
		DRN-S30			<b>27.37 / 0.790</b>	<b>25.25 / 0.651</b>	24.96 / 0.604	<b>22.94 / 0.640</b>	<b>25.29 / 0.804</b>
	50%	CP [101]	2.7	99.4	27.08 / 0.780	25.04 / 0.644	24.72 / 0.600	22.69 / 0.631	25.01 / 0.794
		Thinet [50]			27.18 / 0.783	25.11 / 0.647	24.83 / 0.601	22.77 / 0.633	25.08 / 0.797
		DCP [52]			27.20 / 0.784	25.15 / 0.649	24.89 / 0.602	22.82 / 0.635	25.14 / 0.800
		DRN-S50			<b>27.26 / 0.785</b>	<b>25.14 / 0.648</b>	<b>24.94 / 0.602</b>	<b>22.78 / 0.633</b>	<b>25.13 / 0.799</b>
	70%	CP [101]	1.7	62.5	26.97 / 0.776	24.93 / 0.641	24.67 / 0.596	22.53 / 0.624	24.66 / 0.785
		Thinet [50]			27.01 / 0.777	25.01 / 0.642	24.71 / 0.598	22.58 / 0.626	24.71 / 0.787
		DCP [52]			27.07 / 0.779	25.08 / 0.644	24.81 / 0.599	22.65 / 0.627	24.76 / 0.788
		DRN-S70			<b>27.16 / 0.783</b>	<b>25.13 / 0.646</b>	<b>24.91 / 0.601</b>	<b>22.76 / 0.631</b>	<b>25.07 / 0.796</b>

TABLE 4

The effect of the proposed dual regression learning scheme on super-resolution performance in terms of PSNR score on the five benchmark datasets for  $4\times$  SR.

Model	Dual	Set5	Set14	BSDS100	Urban100	Manga109
DRN-S	$\times$	32.53	28.76	27.68	26.54	31.21
	$\checkmark$	<b>32.68</b>	<b>28.93</b>	<b>27.78</b>	<b>26.84</b>	<b>31.52</b>
DRN-L	$\times$	32.61	28.84	27.72	26.77	31.39
	$\checkmark$	<b>32.74</b>	<b>28.98</b>	<b>27.83</b>	<b>27.03</b>	<b>31.73</b>

equipped with the dual regression learning scheme consistently yield better performance on all five benchmark datasets. These results suggest that our dual regression learning scheme improves the reconstruction of HR images by introducing an additional constraint to reduce the space of the mapping function. We also evaluate the effect of our dual regression learning scheme on other models, *e.g.*, SRResNet [31] based network, which also yields similar results (See more results in the supplementary materials).

## 5.2 Effect of Dual Regression Channel Number Search

We conduct an ablation study to verify the effect of our dual regression channel number search method. To be specific, we evaluate the baseline compression methods on our DRN-S model with a 30% compression ratio for  $4\times$  SR and show the experimental results in Table 5. Let “Manually Designed” denotes the compression method that removes a specific number of channels

TABLE 5

The effect of dual regression channel number search on model compression performance of DRN-S30 for  $4\times$  SR.

Channel Number Policy	Dual	#Params (M)	MAdds (G)	PSNR on Set5
Manually Designed	-	3.4	77.4	32.41
Automatically Searched	$\times$	3.2	74.6	32.49
	$\checkmark$	<b>3.1</b>	<b>72.3</b>	<b>32.60</b>

in each layer (remove 30% channels in each layer). “Automatically Searched” denotes the compression method that automatically searches for the channel numbers of each layer. Compared with the compressed model obtained by “Manually Designed”, the compression models obtained by “Automatically Searched” achieve higher performance with less computational cost. Moreover, with our dual regression channel number search, we are able to obtain a lightweight SR model with better performance.

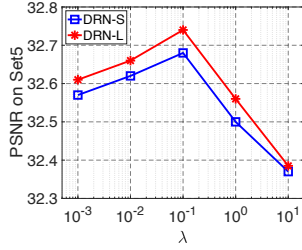
## 5.3 Effect of Dual Regression Channel Pruning

In this part, we investigate the effect of the dual regression channel pruning method. Specifically, we evaluate our methods on our  $4\times$  DRN-S model with compression ratios of 30%, 50%, and 70%. From Table 6, with the dual regression channel pruning method, we are able to obtain lightweight SR models with better performance. Besides, the compressed models obtained by our dual regression channel pruning method consistently achieve higher

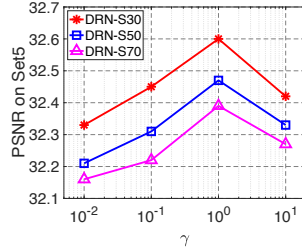


TABLE 6  
The effect of dual regression channel pruning on the model compression performance for  $4\times$  SR.

Compression Ratio	Dual	Set5	Set14	BSDS100	Urban100	Manga109
30%	✗	32.47	28.73	27.60	26.67	31.25
	✓	<b>32.60</b>	<b>28.89</b>	<b>27.76</b>	<b>26.76</b>	<b>31.36</b>
50%	✗	32.38	28.67	27.53	26.56	31.09
	✓	<b>32.47</b>	<b>28.85</b>	<b>27.72</b>	<b>26.62</b>	<b>31.22</b>
70%	✗	32.31	28.65	27.63	26.35	30.88
	✓	<b>32.39</b>	<b>28.74</b>	<b>27.67</b>	<b>26.43</b>	<b>30.94</b>



(a) Effect of  $\lambda$  on SR results.



(b) Effect of  $\gamma$  on pruning results.

Fig. 7. Effect of the hyper-parameters  $\lambda$  and  $\gamma$  on the proposed dual regression learning and dual regression compression method.

SR performance on five benchmark datasets. This experiment demonstrates the effectiveness of our dual regression selection method to obtain efficient SR models.

#### 5.4 Effect of Hyper-parameter $\lambda$ in Eqn. (1)

We conduct an experiment to analyze the effect of the hyper-parameter  $\lambda$  in Eqn. (1), which controls the weight of the dual regression loss. We analyze the effect of  $\lambda$  on the DRN-S and DRN-L models for  $4\times$  SR and compared the model performance on Set5. From Fig. 7(a), when we increase  $\lambda$  from 0.001 to 0.1, the dual regression loss gradually becomes more important and provides powerful supervision. If we further increase  $\lambda$  to 1 or 10, the dual regression loss term would overwhelm the original primal regression loss and hamper the final performance. To obtain a good tradeoff between the primal and dual regression, we set  $\lambda = 0.1$  in practice for the training of all DRN models.

#### 5.5 Effect of Hyper-parameter $\gamma$ in Eqn. (5)

We analyze the effect of the hyper-parameter  $\gamma$  in Eqn. (5), which controls the weight of the dual regression loss on channel pruning. In particular, we investigate the effect of  $\gamma$  on the three compressed models for  $4\times$  SR and compared the model performance on Set5. From Fig. 7(b), the compressed models perform best when  $\gamma$  is set to 1. If we increase or decrease the hyper-parameter  $\gamma$ , the compressed DRN models consistently yield worse SR performance on Set5. Therefore, we set  $\gamma = 1$  in practice to conduct the channel pruning on our DRN models.

#### 5.6 Effect of Dual Regression on HR Data

Actually, we can also add a constraint on the HR domain to reconstruct the original HR images. In this experiment, we investigate the effect of the dual regression loss on HR data and show the results in Table 7. For convenience, we use “DRN-S with dual HR” to represent the model with the regression on both

TABLE 7  
The effect of the dual regression loss on HR data for  $4\times$  SR. DRN-S is taken as the baseline model.

Method	MAdds	Set5	Set14	BSDS100	Urban100	Manga109
DRN-S with dual HR	51.20G	32.69	28.93	27.79	26.85	31.54
DRN-S (Ours)	25.60G	32.68	28.93	27.78	26.84	31.52

LR and HR images. From Table 7, “DRN-S with dual HR” yields approximately  $2\times$  training cost of the original training scheme but very limited performance improvement. Thus, we only apply the dual regression loss to LR data in practice.

## 6 CONCLUSION

In this paper, we have proposed a novel dual regression learning scheme to obtain effective SR models. Specifically, we introduce an additional constraint by reconstructing LR images to reduce the space of possible SR mapping functions. With the proposed learning scheme, we can significantly improve the performance of SR models. Based on the dual regression learning scheme, we further propose a lightweight dual regression compression method to obtain lightweight SR models. We first present a dual regression channel number search method to determine the redundancy of each layer. Based on the searched channel numbers, we then exploit the dual regression scheme to evaluate the importance of channels and prune those redundant ones. Extensive experiments demonstrate the superiority of our method over existing methods.

## ACKNOWLEDGMENTS

This work was partially supported by Ministry of Science and Technology Foundation Project (2020AAA0106900), National Natural Science Foundation of China (62072190, 62072186), Key Realm R&D Program of Guangzhou (202007030007), Fundamental Research Funds for the Central Universities (D2191240), Program for Guangdong Introducing Innovative and Entrepreneurial Teams (2017ZT07X183), Key-Area Research and Development Program of Guangdong Province (2019B010155002), Guangdong Basic and Applied Basic Research Foundation (2019B1515130001), Tencent AI Lab Rhino-Bird Focused Research Program (JR201902), Guangzhou Science and Technology Planning Project (201904010197), Opening Project of Guangdong Key Laboratory of Big Data Analysis and Processing.

## REFERENCES

- [1] K. He, X. Zhang, S. Ren, and J. Sun, “Deep residual learning for image recognition,” in *IEEE Conference on Computer Vision and Pattern Recognition*, 2016, pp. 770–778.
- [2] O. Russakovsky, J. Deng, H. Su, J. Krause, S. Satheesh, S. Ma, Z. Huang, A. Karpathy, A. Khosla, M. Bernstein *et al.*, “Imagenet large scale visual recognition challenge,” *International Journal of Computer Vision*, vol. 115, no. 3, Dec. 2015.
- [3] Z. Wang, D. Liu, J. Yang, W. Han, and T. Huang, “Deep networks for image super-resolution with sparse prior,” in *IEEE International Conference on Computer Vision*, 2015, pp. 370–378.
- [4] W. Dong, P. Wang, W. Yin, G. Shi, F. Wu, and X. Lu, “Denoising prior driven deep neural network for image restoration,” *IEEE Transactions on Pattern Analysis and Machine Intelligence*, vol. 41, no. 10, pp. 2305–2318, Oct. 2019.
- [5] Y. Zhang, Y. Tian, Y. Kong, B. Zhong, and Y. Fu, “Residual dense network for image restoration,” *IEEE Transactions on Pattern Analysis and Machine Intelligence*, Jan. 2020.

- [6] X. Deng and P. L. Dragotti, "Deep convolutional neural network for multi-modal image restoration and fusion," *IEEE Transactions on Pattern Analysis and Machine Intelligence*, Apr. 2020.
- [7] W.-S. Lai, J.-B. Huang, N. Ahuja, and M.-H. Yang, "Fast and accurate image super-resolution with deep laplacian pyramid networks," *IEEE Transactions on Pattern Analysis and Machine Intelligence*, Nov. 2019.
- [8] W. Zhang, Y. Liu, C. Dong, and Y. Qiao, "RankSRGAN: Generative adversarial networks with ranker for image super-resolution," in *IEEE International Conference on Computer Vision*, 2019, pp. 3096–3105.
- [9] X. Hu, H. Mu, X. Zhang, Z. Wang, T. Tan, and J. Sun, "Meta-sr: A magnification-arbitrary network for super-resolution," in *IEEE Conference on Computer Vision and Pattern Recognition*, 2019, pp. 1575–1584.
- [10] S. Anwar and N. Barnes, "Densely residual laplacian super-resolution," *IEEE Transactions on Pattern Analysis and Machine Intelligence*, Sept. 2020.
- [11] S. Zhou, J. Zhang, W. Zuo, and C. C. Loy, "Cross-scale internal graph neural network for image super-resolution," in *Advances in Neural Information Processing Systems*, H. Larochelle, M. Ranzato, R. Hadsell, M. Balcan, and H. Lin, Eds., 2020, pp. 3499–3509.
- [12] X. Kong, H. Zhao, Y. Qiao, and C. Dong, "ClassSR: A general framework to accelerate super-resolution networks by data characteristic," in *Proceedings of the IEEE Conference on Computer Vision and Pattern Recognition*, 2021.
- [13] J. Liang, K. Zhang, S. Gu, L. Van Gool, and R. Timofte, "Flow-based kernel prior with application to blind super-resolution," in *IEEE Conference on Computer Vision and Pattern Recognition*, 2021.
- [14] J. Gu and C. Dong, "Interpreting super-resolution networks with local attribution maps," in *Proceedings of the IEEE Conference on Computer Vision and Pattern Recognition*, 2021.
- [15] D. Ulyanov, A. Vedaldi, and V. Lempitsky, "Deep image prior," in *IEEE Conference on Computer Vision and Pattern Recognition*, 2018, pp. 9446–9454.
- [16] B. Lim, S. Son, H. Kim, S. Nah, and K. M. Lee, "Enhanced deep residual networks for single image super-resolution," in *IEEE Conference on Computer Vision and Pattern Recognition Workshops*, 2017, pp. 136–144.
- [17] Y. Zhang, K. Li, K. Li, L. Wang, B. Zhong, and Y. Fu, "Image super-resolution using very deep residual channel attention networks," in *European Conference on Computer Vision*, 2018, pp. 286–301.
- [18] C. Dong, C. C. Loy, and X. Tang, "Accelerating the super-resolution convolutional neural network," in *European Conference on Computer Vision*. Springer, 2016, pp. 391–407.
- [19] Z. Hui, X. Wang, and X. Gao, "Fast and accurate single image super-resolution via information distillation network," in *IEEE Conference on Computer Vision and Pattern Recognition*, 2018, pp. 723–731.
- [20] Y. Mei, Y. Fan, Y. Zhou, L. Huang, T. S. Huang, and H. Shi, "Image super-resolution with cross-scale non-local attention and exhaustive self-exemplars mining," in *IEEE Conference on Computer Vision and Pattern Recognition*, 2020, pp. 5690–5699.
- [21] B. Niu, W. Wen, W. Ren, X. Zhang, L. Yang, S. Wang, K. Zhang, X. Cao, and H. Shen, "Single image super-resolution via a holistic attention network," in *European Conference on Computer Vision*, 2020, pp. 191–207.
- [22] Y. Guo, J. Chen, J. Wang, Q. Chen, J. Cao, Z. Deng, Y. Xu, and M. Tan, "Closed-loop matters: Dual regression networks for single image super-resolution," in *IEEE Conference on Computer Vision and Pattern Recognition*, 2020, pp. 5407–5416.
- [23] H. Hou and H. Andrews, "Cubic splines for image interpolation and digital filtering," *IEEE Transactions on Acoustics, Speech, and Signal Processing*, vol. 26, no. 6, pp. 508–517, Dec. 1978.
- [24] J. Allebach and P. W. Wong, "Edge-directed interpolation," in *IEEE International Conference on Image Processing*, 1996, pp. 707–710.
- [25] X. Li and M. T. Orchard, "New edge-directed interpolation," *IEEE Transactions on Image Processing*, vol. 10, no. 10, pp. 1521–1527, Oct. 2001.
- [26] N. Nguyen and P. Milanfar, "An efficient wavelet-based algorithm for image superresolution," in *IEEE International Conference on Image Processing*, 2000, pp. 351–354.
- [27] M. Haris, G. Shakhnarovich, and N. Ukita, "Deep back-projection networks for super-resolution," in *IEEE Conference on Computer Vision and Pattern Recognition*, 2018, pp. 1664–1673.
- [28] Z. Li, J. Yang, Z. Liu, X. Yang, G. Jeon, and W. Wu, "Feedback network for image super-resolution," in *IEEE Conference on Computer Vision and Pattern Recognition*, 2019, pp. 3867–3876.
- [29] A. Shocher, N. Cohen, and M. Irani, "“zero-shot” super-resolution using deep internal learning," in *IEEE Conference on Computer Vision and Pattern Recognition*, 2018, pp. 3118–3126.
- [30] J. Gu, H. Lu, W. Zuo, and C. Dong, "Blind super-resolution with iterative kernel correction," in *Proceedings of the IEEE Conference on Computer Vision and Pattern Recognition*, 2019, pp. 1604–1613.
- [31] C. Ledig, L. Theis, F. Huszár, J. Caballero, A. Cunningham, A. Acosta, A. Aitken, A. Tejani, J. Totz, Z. Wang *et al.*, "Photo-realistic single image super-resolution using a generative adversarial network," in *IEEE Conference on Computer Vision and Pattern Recognition*, 2017, pp. 4681–4690.
- [32] T. Tong, G. Li, X. Liu, and Q. Gao, "Image super-resolution using dense skip connections," in *IEEE International Conference on Computer Vision*, 2017, pp. 4809–4817.
- [33] S. Baker and T. Kanade, "Limits on super-resolution and how to break them," *IEEE Transactions on Pattern Analysis and Machine Intelligence*, vol. 24, no. 9, pp. 1167–1183, Sept. 2002.
- [34] M. Ben-Ezra, Z. Lin, and B. Wilburn, "Penrose pixels super-resolution in the detector layout domain," in *IEEE International Conference on Computer Vision*, 2007, pp. 1–8.
- [35] Z. Lin and H.-Y. Shum, "Fundamental limits of reconstruction-based superresolution algorithms under local translation," *IEEE Transactions on Pattern Analysis and Machine Intelligence*, vol. 26, no. 1, pp. 83–97, Jan. 2004.
- [36] C. Dong, C. C. Loy, K. He, and X. Tang, "Learning a deep convolutional network for image super-resolution," in *European Conference on Computer Vision*. Springer, 2014, pp. 184–199.
- [37] —, "Image super-resolution using deep convolutional networks," *IEEE Transactions on Pattern Analysis and Machine Intelligence*, vol. 38, no. 2, pp. 295–307, Feb. 2016.
- [38] J. Kim, J. Kwon Lee, and K. Mu Lee, "Accurate image super-resolution using very deep convolutional networks," in *IEEE Conference on Computer Vision and Pattern Recognition*, 2016, pp. 1646–1654.
- [39] X. Mao, C. Shen, and Y.-B. Yang, "Image restoration using very deep convolutional encoder-decoder networks with symmetric skip connections," in *Advances in Neural Information Processing Systems*, 2016, pp. 2802–2810.
- [40] K. Zhang, W. Zuo, and L. Zhang, "Learning a single convolutional super-resolution network for multiple degradations," in *IEEE Conference on Computer Vision and Pattern Recognition*, 2018, pp. 3262–3271.
- [41] Y. Zhang, Y. Tian, Y. Kong, B. Zhong, and Y. Fu, "Residual dense network for image super-resolution," in *IEEE Conference on Computer Vision and Pattern Recognition*, 2018, pp. 2472–2481.
- [42] Y. Guo, Y. Luo, Z. He, J. Huang, and J. Chen, "Hierarchical neural architecture search for single image super-resolution," *IEEE Signal Processing Letters*, vol. 27, pp. 1255–1259, 2020.
- [43] J. Liang, J. Cao, G. Sun, K. Zhang, L. Van Gool, and R. Timofte, "Swinir: Image restoration using swin transformer," in *IEEE International Conference on Computer Vision Workshops*, 2021.
- [44] X. Zhang, H. Zeng, and L. Zhang, "Edge-oriented convolution block for real-time super resolution on mobile devices," in *Proceedings of the ACM International Conference on Multimedia*, 2021.
- [45] Q. Gao, Y. Zhao, G. Li, and T. Tong, "Image super-resolution using knowledge distillation," in *Asian Conference on Computer Vision*, 2018, pp. 527–541.
- [46] W. Lee, J. Lee, D. Kim, and B. Ham, "Learning with privileged information for efficient image super-resolution," in *European Conference on Computer Vision*, 2020, pp. 465–482.
- [47] Y. Zhang, H. Chen, X. Chen, Y. Deng, C. Xu, and Y. Wang, "Data-free knowledge distillation for image super-resolution," in *IEEE Conference on Computer Vision and Pattern Recognition*, 2021, pp. 7852–7861.
- [48] S. Han, J. Pool, J. Tran, and W. Dally, "Learning both weights and connections for efficient neural network," in *Advances in Neural Information Processing Systems*, 2015, pp. 1135–1143.
- [49] S. Han, H. Mao, and W. J. Dally, "Deep compression: Compressing deep neural network with pruning, trained quantization and Huffman coding," in *International Conference on Learning Representations*, 2016, pp. 1–14.
- [50] J. Luo, H. Zhang, H. Zhou, C. Xie, J. Wu, and W. Lin, "Thinet: Pruning cnn filters for a thinner net," *IEEE Transactions on Pattern Analysis and Machine Intelligence*, vol. 41, no. 10, pp. 2525–2538, Oct. 2019.
- [51] Y. Guo, Y. Zheng, M. Tan, Q. Chen, Z. Li, J. Chen, P. Zhao, and J. Huang, "Towards accurate and compact architectures via neural architecture transformer," *IEEE Transactions on Pattern Analysis and Machine Intelligence*, 2021.

- [52] Z. Zhuangwei, T. Mingkui, Z. Bohan, J. Liu, Y. Guo, Q. Wu, J. Huang, and J. Zhu, "Discrimination-aware channel pruning for deep neural networks," in *Advances in Neural Information Processing Systems*, 2018, pp. 883–894.
- [53] M. Lin, R. Ji, Y. Wang, Y. Zhang, B. Zhang, Y. Tian, and L. Shao, "HRank: Filter pruning using high-rank feature map," in *IEEE Conference on Computer Vision and Pattern Recognition*, 2020, pp. 1529–1538.
- [54] Z. Liu, H. Mu, X. Zhang, Z. Guo, X. Yang, K.-T. Cheng, and J. Sun, "Metapruning: Meta learning for automatic neural network channel pruning," in *IEEE Conference on Computer Vision and Pattern Recognition*, 2019, pp. 3296–3305.
- [55] X. Dong and Y. Yang, "Network pruning via transformable architecture search," in *Advances in Neural Information Processing Systems*, 2019, pp. 759–770.
- [56] M. Lin, R. Ji, Y. Zhang, B. Zhang, Y. Wu, and Y. Tian, "Channel pruning via automatic structure search," in *Proceedings of the International Joint Conference on Artificial Intelligence*, 2020, pp. 673–679.
- [57] J. Wang, H. Bai, J. Wu, X. Shi, J. Huang, I. King, M. Lyu, and J. Cheng, "Revisiting parameter sharing for automatic neural channel number search," 2020, pp. 5991–6002.
- [58] J. Frankle and M. Carbin, "The lottery ticket hypothesis: Finding sparse, trainable neural networks," *arXiv preprint arXiv:1803.03635*, 2018.
- [59] Y. Guo, D. Stutz, and B. Schiele, "Improving robustness by enhancing weak subnets," in *European Conference on Computer Vision*. Springer, 2022.
- [60] V. Sehwag, S. Wang, P. Mittal, and S. Jana, "On pruning adversarially robust neural networks," 2020.
- [61] B. Li, S. Wang, Y. Jia, Y. Lu, Z. Zhong, L. Carin, and S. Jana, "Towards practical lottery ticket hypothesis for adversarial training," *arXiv preprint arXiv:2003.05733*, 2020.
- [62] Y. Li, S. Gu, K. Zhang, L. Van Gool, and R. Timofte, "DHP: differentiable meta pruning via hypernetworks," in *European Conference on Computer Vision*, 2020, pp. 608–624.
- [63] J. Xin, N. Wang, X. Jiang, J. Li, H. Huang, and X. Gao, "Binarized neural network for single image super resolution," in *European Conference on Computer Vision*, 2020, pp. 91–107.
- [64] Y. Ma, H. Xiong, Z. Hu, and L. Ma, "Efficient super resolution using binarized neural network," in *IEEE Conference on Computer Vision and Pattern Recognition Workshops*, 2019, pp. 694–703.
- [65] H. Li, C. Yan, S. Lin, X. Zheng, Y. Li, B. Zhang, F. Yang, and R. Ji, "PAMS: quantized super-resolution via parameterized max scale," in *European Conference on Computer Vision*, 2020, pp. 564–580.
- [66] D. He, Y. Xia, T. Qin, L. Wang, N. Yu, T. Liu, and W.-Y. Ma, "Dual learning for machine translation," in *Advances in Neural Information Processing Systems*, 2016, pp. 820–828.
- [67] Y. Xia, T. Qin, W. Chen, J. Bian, N. Yu, and T.-Y. Liu, "Dual supervised learning," in *International Conference on Machine Learning*, 2017, pp. 3789–3798.
- [68] Y. Xia, X. Tan, F. Tian, T. Qin, N. Yu, and T.-Y. Liu, "Model-level dual learning," in *International Conference on Machine Learning*, 2018, pp. 5383–5392.
- [69] Y. Zhang, T. Xiang, T. M. Hospedales, and H. Lu, "Deep mutual learning," in *IEEE Conference on Computer Vision and Pattern Recognition*, 2018, pp. 4320–4328.
- [70] J.-Y. Zhu, T. Park, P. Isola, and A. A. Efros, "Unpaired image-to-image translation using cycle-consistent adversarial networks," in *IEEE International Conference on Computer Vision*, 2017, pp. 2223–2232.
- [71] Z. Yi, H. Zhang, P. T. Gong *et al.*, "DualGAN: Unsupervised dual learning for image-to-image translation," in *IEEE International Conference on Computer Vision*, 2017, pp. 2849–2857.
- [72] J. Cao, Y. Guo, Q. Wu, C. Shen, J. Huang, and M. Tan, "Adversarial learning with local coordinate coding," in *International Conference on Machine Learning*, pp. 707–715.
- [73] Y. Guo, Q. Chen, J. Chen, Q. Wu, Q. Shi, and M. Tan, "Auto-embedding generative adversarial networks for high resolution image synthesis," *IEEE Transactions on Multimedia*, Nov. 2019.
- [74] M. Mohri, A. Rostamizadeh, and A. Talwalkar, *Foundations of machine learning*. MIT Press, 2012.
- [75] H. Hao, A. Kadav, I. Durdanovic, H. Samet, and H. P. Graf, "Pruning filters for efficient convnets," in *International Conference on Learning Representations*, 2017, pp. 1–13.
- [76] Y. He, G. Kang, X. Dong, Y. Fu, and Y. Yang, "Soft filter pruning for accelerating deep convolutional neural networks," in *Proceedings of the International Joint Conference on Artificial Intelligence*, 2018, pp. 2234–2240.
- [77] Y. He, J. Lin, Z. Liu, H. Wang, L.-J. Li, and S. Han, "Amc: Automl for model compression and acceleration on mobile devices," in *European Conference on Computer Vision*, 2018, pp. 784–800.
- [78] H. Liu, K. Simonyan, and Y. Yang, "DARTS: differentiable architecture search," in *International Conference on Learning Representations*, 2019, pp. 1–13.
- [79] J.-H. Luo, J. Wu, and W. Lin, "Thinet: A filter level pruning method for deep neural network compression," in *IEEE International Conference on Computer Vision*, 2017, pp. 5058–5066.
- [80] S. Bahmani, B. Raj, and P. T. Boufounos, "Greedy sparsity-constrained optimization," *Journal of Machine Learning Research*, vol. 14, no. Mar, pp. 807–841, 2013.
- [81] J. Liu, B. Zhuang, Z. Zhuang, Y. Guo, J. Huang, J. Zhu, and M. Tan, "Discrimination-aware network pruning for deep model compression," *arXiv preprint arXiv:2001.01050*, 2020.
- [82] C. Dong, C. C. Loy, K. He, and X. Tang, "Image super-resolution using deep convolutional networks," *IEEE Transactions on Pattern Analysis and Machine Intelligence*, vol. 38, no. 2, pp. 295–307, 2016.
- [83] W. Shi, J. Caballero, F. Huszar, J. Totz, A. P. Aitken, R. Bishop, D. Rueckert, and Z. Wang, "Real-time single image and video super-resolution using an efficient sub-pixel convolutional neural network," in *IEEE Conference on Computer Vision and Pattern Recognition*, 2016, pp. 1874–1883.
- [84] W.-S. Lai, J.-B. Huang, N. Ahuja, and M.-H. Yang, "Deep laplacian pyramid networks for fast and accurate super-resolution," in *IEEE Conference on Computer Vision and Pattern Recognition*, 2017, pp. 624–632.
- [85] Y. Tai, J. Yang, and X. Liu, "Image super-resolution via deep recursive residual network," in *IEEE Conference on Computer Vision and Pattern Recognition*, 2017, pp. 3147–3155.
- [86] N. Ahn, B. Kang, and K.-A. Sohn, "Fast, accurate, and lightweight super-resolution with cascading residual network," in *European Conference on Computer Vision*, 2018, pp. 252–268.
- [87] Z. Hui, X. Gao, Y. Yang, and X. Wang, "Lightweight image super-resolution with information multi-distillation network," in *Proceedings of the ACM International Conference on Multimedia*, 2019, pp. 2024–2032.
- [88] H. Zhao, X. Kong, J. He, Y. Qiao, and C. Dong, "Efficient image super-resolution using pixel attention," in *European Conference on Computer Vision Workshops*, 2020, pp. 56–72.
- [89] T. Dai, J. Cai, Y. Zhang, S.-T. Xia, and L. Zhang, "Second-order attention network for single image super-resolution," in *IEEE Conference on Computer Vision and Pattern Recognition*, 2019, pp. 11 065–11 074.
- [90] X. Wang, K. Yu, S. Wu, J. Gu, Y. Liu, C. Dong, Y. Qiao, and C. Change Loy, "ESRGAN: Enhanced super-resolution generative adversarial networks," in *European Conference on Computer Vision Workshops*, 2018, pp. 63–79.
- [91] Z. Iqbal, D. Nguyen, G. Hangel, S. Motyka, W. Bogner, and S. Jiang, "Super-resolution 1h magnetic resonance spectroscopic imaging utilizing deep learning," *Frontiers in oncology*, vol. 9, Oct. 2019.
- [92] O. Ronneberger, P. Fischer, and T. Brox, "U-Net: Convolutional networks for biomedical image segmentation," in *International Conference on Medical Image Computing and Computer-Assisted Intervention*, 2015, pp. 234–241.
- [93] R. Timofte, E. Agustsson, L. Van Gool, M.-H. Yang, L. Zhang, B. Lim, S. Son, H. Kim, S. Nah, K. M. Lee *et al.*, "Ntire 2017 challenge on single image super-resolution: Methods and results," in *IEEE Conference on Computer Vision and Pattern Recognition Workshops*. IEEE, 2017, pp. 1110–1121.
- [94] M. Bevilacqua, A. Roumy, C. Guillemot, and M. Alberi-Morel, "Low-complexity single-image super-resolution based on nonnegative neighbor embedding," in *British Machine Vision Conference*, 2012, pp. 1–10.
- [95] R. Zeyde, M. Elad, and M. Protter, "On single image scale-up using sparse-representations," in *International Conference on Curves and Surfaces*. Springer, 2010, pp. 711–730.
- [96] P. Arbelaez, M. Maire, C. Fowlkes, and J. Malik, "Contour detection and hierarchical image segmentation," *IEEE Transactions on Pattern Analysis and Machine Intelligence*, vol. 33, no. 5, pp. 898–916, May 2011.
- [97] J.-B. Huang, A. Singh, and N. Ahuja, "Single image super-resolution from transformed self-exemplars," in *IEEE Conference on Computer Vision and Pattern Recognition*, 2015, pp. 5197–5206.
- [98] Y. Matsui, K. Ito, Y. Aramaki, A. Fujimoto, T. Ogawa, T. Yamasaki, and K. Aizawa, "Sketch-based manga retrieval using manga109 dataset," *Multimedia Tools and Applications*, vol. 76, no. 20, Oct. 2017.
- [99] Z. Wang, A. C. Bovik, H. R. Sheikh, and E. P. Simoncelli, "Image quality assessment: from error visibility to structural similarity," *IEEE*

- Transactions on Image Processing*, vol. 13, no. 4, pp. 600–612, Apr. 2004.
- [100] D. Kingma and J. Ba, “Adam: A method for stochastic optimization,” in *International Conference on Learning Representations*, 2015, pp. 1–15.
  - [101] Y. He, X. Zhang, and J. Sun, “Channel pruning for accelerating very deep neural networks,” in *IEEE International Conference on Computer Vision*, 2017, pp. 1389–1397.
  - [102] Y. Yuan, S. Liu, J. Zhang, Y. Zhang, C. Dong, and L. Lin, “Unsupervised image super-resolution using cycle-in-cycle generative adversarial networks,” in *IEEE Conference on Computer Vision and Pattern Recognition Workshops*, 2018, pp. 701–710.
  - [103] T. Zhao, C. Zhang, W. Ren, D. Ren, and Q. Hu, “Unsupervised degradation learning for single image super-resolution,” *arXiv preprint arXiv:1812.04240*, 2018.
  - [104] A. L. Maas, A. Y. Hannun, and A. Y. Ng, “Rectifier nonlinearities improve neural network acoustic models,” in *International Conference on Machine Learning*, vol. 30, no. 1, 2013, p. 3.
  - [105] R. A. Amjad and B. C. Geiger, “Learning representations for neural network-based classification using the information bottleneck principle,” *IEEE Transactions on Pattern Analysis and Machine Intelligence*, Sept. 2019.
  - [106] B. Zhou, A. Lapedriza, A. Khosla, A. Oliva, and A. Torralba, “Places: A 10 million image database for scene recognition,” *IEEE Transactions on Pattern Analysis and Machine Intelligence*, vol. 40, no. 6, pp. 1452–1464, Jun. 2017.



# Supplementary Materials for “Towards Lightweight Super-Resolution with Dual Regression Learning”

We organize our supplementary materials as follows. First, we provide the derivation of the generalization error bound for the dual regression scheme in Section A. Second, we propose a dual regression adaptation algorithm for unpaired real-world images in Section B. Then, we provide more details about the architecture design of the proposed DRN model in Section C. Last, we provide more experimental results on the dual regression learning scheme on the SR tasks with paired data and unpaired data in Section D and Section E.

## APPENDIX A THEORETICAL ANALYSIS

In this section, we will analyze the generalization bound for the proposed method. The generalization error of the dual learning scheme is to measure how accurately the algorithm predicts for the unseen test data in the primal and dual tasks. Firstly, we will introduce the definition of the generalization error as follows:

**Definition 3** *Given an underlying distribution  $\mathcal{S}$  and hypotheses  $P \in \mathcal{P}$  and  $D \in \mathcal{D}$  for the primal and dual tasks, where  $\mathcal{P} = \{P_{\theta_{xy}}(\mathbf{x}); \theta_{xy} \in \Theta_{xy}\}$  and  $\mathcal{D} = \{D_{\theta_{yx}}(\mathbf{y}); \theta_{yx} \in \Theta_{yx}\}$ , and  $\Theta_{xy}$  and  $\Theta_{yx}$  are parameter spaces, respectively, the generalization error (expected loss) is defined by:*

$$E(P, D) = \mathbb{E}_{(\mathbf{x}, \mathbf{y}) \sim \mathcal{P}} [\mathcal{L}_P(P(\mathbf{x}), \mathbf{y}) + \lambda \mathcal{L}_D(D(P(\mathbf{x})), \mathbf{x})], \forall P \in \mathcal{P}, D \in \mathcal{D}.$$

In practice, the goal of the dual learning is to optimize the bi-directional tasks. For any  $P \in \mathcal{P}$  and  $D \in \mathcal{D}$ , we define the empirical loss on the  $N$  samples as follows:

$$\hat{E}(P, D) = \frac{1}{N} \sum_{i=1}^N \mathcal{L}_P(P(\mathbf{x}_i), \mathbf{y}_i) + \lambda \mathcal{L}_D(D(P(\mathbf{x}_i)), \mathbf{x}_i). \quad (6)$$

Following [74], we define Rademacher complexity for dual learning in this paper. We define the function space as  $\mathcal{H}_{dual} \in \mathcal{P} \times \mathcal{D}$ , this Rademacher complexity can measure the complexity of the function space, that is it can capture the richness of a family of the primal and the dual models. For our application, we mildly rewrite the definition of Rademacher complexity in [74] as follows:

**Definition 4 (Rademacher complexity of dual learning)** *Given an underlying distribution  $\mathcal{S}$ , and its empirical distribution  $\mathcal{Z} = \{\mathbf{z}_1, \mathbf{z}_2, \dots, \mathbf{z}_N\}$ , where  $\mathbf{z}_i = (\mathbf{x}_i, \mathbf{y}_i)$ , then the Rademacher complexity of dual learning is defined as:*

$$R_N^{DL}(\mathcal{H}_{dual}) = \mathbb{E}_{\mathcal{Z}} [\hat{R}_{\mathcal{Z}}(P, D)], \forall P \in \mathcal{P}, D \in \mathcal{D},$$

where  $\hat{R}_{\mathcal{Z}}(P, D)$  is the empirical Rademacher complexity defined as:

$$\hat{R}_{\mathcal{Z}}(P, D) = \mathbb{E}_{\sigma} \left[ \sup_{(P, D) \in \mathcal{H}_{dual}} \frac{1}{N} \sum_{i=1}^N \sigma_i (\mathcal{L}_P(P(\mathbf{x}_i), \mathbf{y}_i) + \lambda \mathcal{L}_D(D(P(\mathbf{x}_i)), \mathbf{x}_i)) \right].$$

where  $\sigma = \{\sigma_1, \sigma_2, \dots, \sigma_N\}$  are independent uniform  $\{\pm 1\}$ -valued random variables with  $p(\sigma_i=1) = p(\sigma_i=-1) = \frac{1}{2}$ .

Based on the above definitions, we analyze the generalization bound for the proposed dual regression scheme.

**Theorem 2** *Let  $\mathcal{L}_P(P(\mathbf{x}), \mathbf{y}) + \lambda \mathcal{L}_D(D(P(\mathbf{x})), \mathbf{x})$  be a mapping from  $\mathcal{X} \times \mathcal{Y}$  to  $[0, 1]$ , and the function space  $\mathcal{H}_{dual}$  be infinite. Then, for any  $\delta > 0$ , with probability at least  $1 - \delta$ , the generalization error  $E(P, D)$  (i.e., expected loss) satisfies for all  $(P, D) \in \mathcal{H}_{dual}$ :*

$$E(P, D) \leq \hat{E}(P, D) + 2\hat{R}_{\mathcal{Z}}^{DL}(\mathcal{H}_{dual}) + 3\sqrt{\frac{1}{2N} \log \left( \frac{2}{\delta} \right)}, \quad (7)$$

where  $N$  is the number of samples and  $\hat{R}_{\mathcal{Z}}^{DL}$  is the empirical Rademacher complexity of dual learning. Let  $\mathcal{B}(P, D)$  be the generalization bound of the dual regression SR, i.e.,  $\mathcal{B}(P, D) = 2\hat{R}_{\mathcal{Z}}^{DL}(\mathcal{H}_{dual}) + 3\sqrt{\frac{1}{2N} \log \left( \frac{2}{\delta} \right)}$ , we have

$$\mathcal{B}(P, D) \leq \mathcal{B}(P), \quad (8)$$

where  $\mathcal{B}(P)$ ,  $P \in \mathcal{H}$  is the generalization bound of standard supervised learning w.r.t. the Rademacher complexity  $\hat{R}_{\mathcal{Z}}^{SL}(\mathcal{H})$ .

**Proof** Based on Theorem 3.3 in [74], we have the generalization bound in (7). According to the definition of Rademacher complexity, we have  $\hat{R}_{\mathcal{Z}}^{DL}(\mathcal{H}_{dual}) \leq \hat{R}_{\mathcal{Z}}^{SL}(\mathcal{H})$  because the capacity of the function space  $\mathcal{H}_{dual} \in \mathcal{P} \times \mathcal{D}$  is smaller than the capacity of the function space  $\mathcal{H} \in \mathcal{P}$ . With the same number of samples, we have  $\mathcal{B}(P, D) \leq \mathcal{B}(P)$ .  $\square$

**Algorithm 2:** Adaptation Algorithm on Unpaired Data.

---

**Input:** Unpaired real-world data:  $\mathcal{S}_U$ ;  
 Paired synthetic data:  $\mathcal{S}_P$ ;  
 Batch sizes for  $\mathcal{S}_U$  and  $\mathcal{S}_P$ :  $m$  and  $n$ ;  
 Indicator function:  $\mathbf{1}_{\mathcal{S}_P}(\cdot)$ .

```

1 Load the pretrained models  $P$  and  $D$ .
2 while not convergent do
3   Sample unlabeled data  $\{\mathbf{x}_i\}_{i=1}^m$  from  $\mathcal{S}_U$ ;
4   Sample labeled data  $\{(\mathbf{x}_i, \mathbf{y}_i)\}_{i=m+1}^{m+n}$  from  $\mathcal{S}_P$ ;
5   // Update the primal model
6   Update  $P$  by minimizing the objective:
7      $\sum_{i=1}^{m+n} \mathbf{1}_{\mathcal{S}_P}(\mathbf{x}_i) \mathcal{L}_P(P(\mathbf{x}_i), \mathbf{y}_i) + \lambda \mathcal{L}_D(D(P(\mathbf{x}_i)), \mathbf{x}_i)$ 
8   // Update the dual model
9   Update  $D$  by minimizing the objective:
10     $\sum_{i=1}^{m+n} \lambda \mathcal{L}_D(D(P(\mathbf{x}_i)), \mathbf{x}_i)$ 
11 end
```

---

Theorem 2 shows that with probability at least  $1 - \delta$ , the generalization error is smaller than  $2\hat{R}_{\mathcal{Z}}^{DL} + 3\sqrt{\frac{1}{2N} \log(\frac{2}{\delta})}$ . It suggests that using the function space with larger capacity and more samples can guarantee better generalization. Note that this generalization bound is tight when training data are sufficient, and the primal and dual models are powerful enough.

**Remark 1** Based on the definition of Rademacher complexity, the capacity of the function space  $\mathcal{H}_{dual} \in \mathcal{P} \times \mathcal{D}$  is smaller than the capacity of the function space  $\mathcal{H} \in \mathcal{P}$  or  $\mathcal{H} \in \mathcal{D}$  in traditional supervised learning, i.e.,  $\hat{R}_{\mathcal{Z}}^{DL} \leq \hat{R}_{\mathcal{Z}}^{SL}$ , where  $\hat{R}_{\mathcal{Z}}^{SL}$  is Rademacher complexity defined in supervised learning. In other words, dual learning has a smaller generalization bound than supervised learning and the proposed dual regression model helps the primal model to achieve more accurate SR predictions.

## APPENDIX B

### DUAL REGRESSION LEARNING SCHEME FOR UNPAIRED DATA

Most SR methods rely on the paired training data, i.e., HR images with their Bicubic-degraded LR counterparts. However, the real-world data with unknown degradation methods often do not have the same distribution as the LR images obtained by a specific degradation method (e.g., Bicubic). In these cases, if we directly apply existing SR models to real-world data, they often incur a severe adaptation problem and yield poor performance [102], [103]. To address this issue, we propose a dual regression adaptation method to adapt SR models to the real-world LR data, e.g., raw video frames from YouTube.

#### B.1 Dual Regression Scheme for Unpaired Data

We consider a more general SR case where there are no corresponding HR data w.r.t. the real-world LR data. More critically, the degradation methods of LR images are often unknown, making this problem very challenging. In this case, existing SR models often incur a severe adaptation problem [102], [103]. To alleviate this issue, we propose an efficient algorithm to adapt SR models to the new LR data. The training algorithm is shown in Algorithm 2.

Note that the dual regression mapping learns the underlying degradation methods and does not necessarily depend on HR images. Thus, we can use it to directly learn from the unpaired real-world LR data to perform model adaptation. To ensure the reconstruction performance of HR images, we also incorporate the information from paired synthetic data that can be obtained very easily (e.g., using the Bicubic kernel). Given  $M$  unpaired LR samples and  $N$  paired synthetic samples, the objective function can be written as:

$$\sum_{i=1}^{M+N} \mathbf{1}_{\mathcal{S}_P}(\mathbf{x}_i) \mathcal{L}_P(P(\mathbf{x}_i), \mathbf{y}_i) + \lambda \mathcal{L}_D(D(P(\mathbf{x}_i)), \mathbf{x}_i), \quad (9)$$

where  $\mathbf{1}_{\mathcal{S}_P}(\mathbf{x}_i)$  is an indicator function that equals 1 when  $\mathbf{x}_i \in \mathcal{S}_P$ ; otherwise, the function equals 0.

#### B.2 Training Methods

In this section, we introduce the training methods of the dual regression scheme on paired and unpaired data. In the paired data case, only the paired LR and HR images are used as labels to train the dual regression network. However, in the unpaired data case, both the paired and unpaired LR data are used to train the model. Note that with the dual regression scheme, the paired data are used to boost the training of the models on the unpaired data case.

**Training method on paired data.** Given paired training data, we follow the learning scheme of supervised SR methods [16], [27] and train our models by minimizing Eqn. (1). Specifically, the paired LR and HR images are both used as labels to train the proposed

dual regression network. As shown in Figure 1, the ground-truth HR images are used to guide the primal regression model to learn the mapping  $LR \rightarrow HR$ . In addition, the LR images are used to guide the dual regression model to estimate the degradation kernel, which reduces the possible function space in super-resolution. With the dual regression scheme, we are able to find a good mapping to reconstruct HR images from LR images (see the results in Table 1 and Table 2).

**Training method on unpaired data.** As shown in Algorithm 2, for each iteration, we first sample  $m$  unpaired real-world data from  $\mathcal{S}_U$  and  $n$  paired synthetic data from  $\mathcal{S}_P$ , respectively. Then, we train our model in an end-to-end manner by minimizing the objective in Eqn. (9). For convenience, we define the data ratio of unpaired data as

$$\rho = m/(m + n). \quad (10)$$

Since paired synthetic data can be obtained very easily (*e.g.*, using the Bicubic kernel to produce LR-HR pairs), we can adjust  $\rho$  by changing the number of paired synthetic samples  $n$ . In practice, we set  $\rho = 30\%$  to obtain the best results (see the discussions in Section E.4). With the proposed dual regression scheme, we can adapt SR models to the various unpaired data while preserving good reconstruction performance (see the results in Section E).

## APPENDIX C

### MORE DETAILS OF THE DUAL REGRESSION NETWORK

In this section, we provide more details about the dual regression network. First, we depict the architecture of our dual regression network (DRN) and show the detailed architecture in Fig. A. Then, we provide more implementation details of the dual regression network, such as the depth and width of the dual regression network architecture.

#### C.1 Architecture Design of DRN

We build our DRN based on the design of U-Net for super-resolution [91], [92] (see Fig. A). Our DRN model consists of two parts: a primal network and a dual network. We present the details for each network as follows.

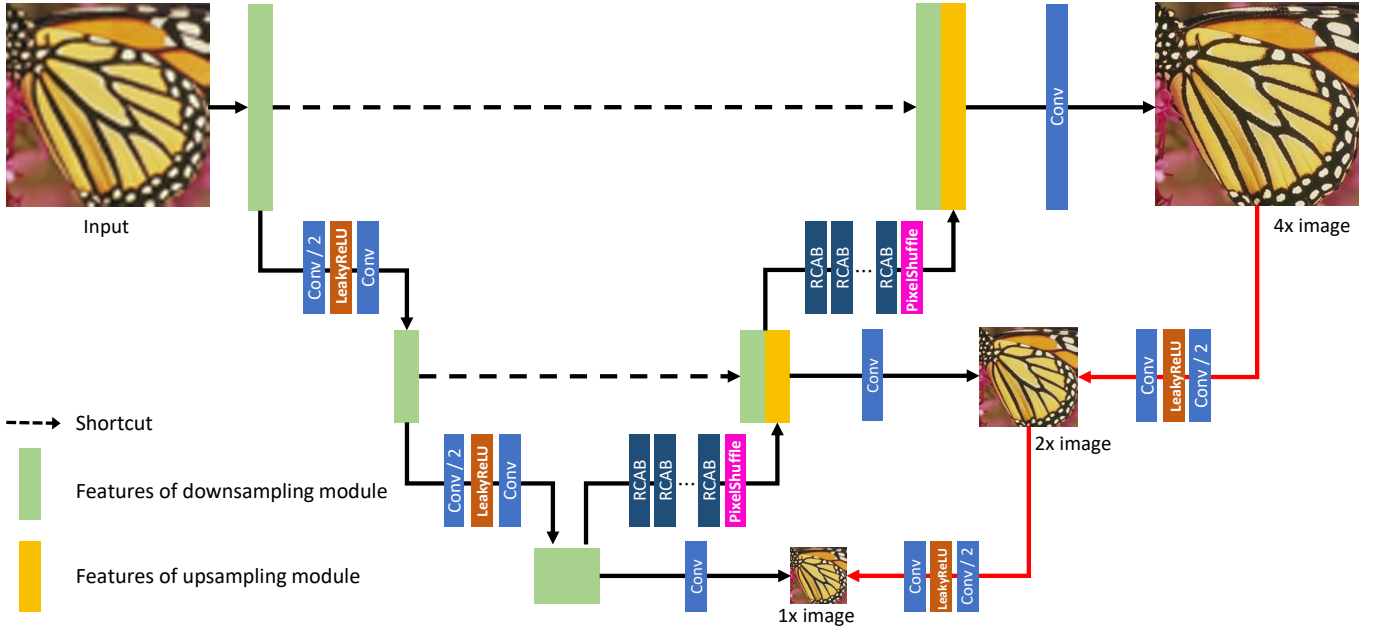


Fig. A. The architecture of DRN for  $4\times$  SR. DRN contains a primal network and a dual network (marked as red lines). The green box denotes the feature maps of the downsampling module (left half) while the yellow box refers to the feature maps of the upsampling module (right half). Following U-Net, we concatenate the corresponding shallow and deep feature maps via shortcut connections.

The primal network follows the downsampling-upsampling design of U-Net. Both the downsampling (left half of Fig. A) and upsampling (right half of Fig. A) modules contain  $\log_2(s)$  basic blocks, where  $s$  denotes the scale factor. This implies that the network will have 2 blocks for  $4\times$  upscaling (see Fig. A) and 3 blocks for  $8\times$  upscaling. Unlike the baseline U-Net, we build each basic block using  $B$  residual channel attention blocks (RCAB) [17] to improve the model capacity. Following [3], [84], we add additional outputs to produce images at the corresponding scale (*i.e.*,  $1\times$ ,  $2\times$ , and  $4\times$  images) and apply the proposed loss to them to train the model. Note that we use the Bicubic kernel to upscale LR images before feeding them into the primal network. Please refer to the supplementary materials for more details.

We design a dual network to produce the downsampled LR images from the super-resolved images (see red lines in Fig. A). Note that the dual task aims to learn a downsampling operation, which is much simpler than the primal task for learning the upscaling mapping. Thus, we design the dual model with only two convolution layers and a LeakyReLU activation layer [104], which has much lower computational cost than the primal model but works well in practice (see the results in Section 4).

## C.2 Model Details of Dual Regression Network

Deep neural networks (DNNs) have achieved great success in image classification [1], [105], [106], image generation [72], and image restoration [16], [17]. In this paper, we propose a novel Dual Regression Network (DRN), which contains a primal model and a dual model. Specifically, the primal model contains 2 basic blocks for  $4\times$  SR and 3 blocks for  $8\times$  SR. To form a closed-loop, according to the architecture design of the primal model, there are 2 dual models for  $4\times$  SR and 3 dual models for  $8\times$  SR, respectively.

Let  $B$  be the number of RCABs [17] and  $F$  be the number of base feature channels. For  $4\times$  SR, we set  $B = 30$  and  $F = 16$  for DRN-S and  $B = 40$  and  $F = 20$  for DRN-L. For  $8\times$  SR, we set  $B = 30$  and  $F = 8$  for DRN-S and  $B = 36$  and  $F = 10$  for DRN-L. Moreover, we set the reduction ratio  $r = 16$  in all RCABs for our DRN model and set the negative slope to 0.2 for all LeakyReLU in DRN. We show the detailed architecture of the  $8\times$  DRN model in Table A. To obtain the  $4\times$  model, one can simply remove one basic block from the  $8\times$  model.

As shown in Table A, we use Conv(1,1) and Conv(3,3) to represent the convolution layer with the kernel size of  $1 \times 1$  and  $3 \times 3$ , respectively. We use Conv<sub>s2</sub> to represent the convolution layer with the stride of 2. Following the settings of EDSR [16], we build the Upsampler with one convolution layer and one pixel-shuffle [83] layer to upscale the feature maps. Moreover, we use h and w to represent the height and width of the input LR images. Thus, the shape of output images should be  $8h \times 8w$  for the  $8\times$  model.

TABLE A  
Detailed model design of the proposed  $8\times$  DRN.

Module	Module details	Input shape	Output shape
Head	Conv(3,3)	(3, 8h, 8w)	(1F, 8h, 8w)
Down 1	Conv <sub>s2</sub> -LeakyReLU-Conv	(1F, 8h, 8w)	(2F, 4h, 4w)
Down 2	Conv <sub>s2</sub> -LeakyReLU-Conv	(2F, 4h, 4w)	(4F, 2h, 2w)
Down 3	Conv <sub>s2</sub> -LeakyReLU-Conv	(4F, 2h, 2w)	(8F, 1h, 1w)
Up 1	$B$ RCABs	(8F, 1h, 1w)	(8F, 1h, 1w)
	$2\times$ Upsampler	(8F, 1h, 1w)	(8F, 2h, 2w)
	Conv(1,1)	(8F, 2h, 2w)	(4F, 2h, 2w)
Concatenation 1	Concatenation of the output of Up 1 and Down 2	$(4F, 2h, 2w) \oplus (4F, 2h, 2w)$	(8F, 2h, 2w)
Up 2	$B$ RCABs	(8F, 2h, 2w)	(8F, 2h, 2w)
	$2\times$ Upsampler	(8F, 2h, 2w)	(8F, 4h, 4w)
	Conv(1,1)	(8F, 4h, 4w)	(2F, 4h, 4w)
Concatenation 2	Concatenation of the output of Up 2 and Down 1	$(2F, 4h, 4w) \oplus (2F, 4h, 4w)$	(4F, 4h, 4w)
Up 3	$B$ RCABs	(4F, 4h, 4w)	(4F, 4h, 4w)
	$2\times$ Upsampler	(4F, 4h, 4w)	(4F, 8h, 8w)
	Conv(1,1)	(4F, 8h, 8w)	(1F, 8h, 8w)
Concatenation 3	Concatenation of the output of Up3 and Head	$(1F, 8h, 8w) \oplus (1F, 8h, 8w)$	(2F, 8h, 8w)
Tail 0	Conv(3,3)	(8F, 1h, 1w)	(3, 1h, 1w)
Tail 1	Conv(3,3)	(8F, 2h, 2w)	(3, 2h, 2w)
Tail 2	Conv(3,3)	(4F, 4h, 4w)	(3, 4h, 4w)
Tail 3	Conv(3,3)	(2F, 8h, 8w)	(3, 8h, 8w)
Dual 1	Conv <sub>s2</sub> -LeakyReLU-Conv	(3, 8h, 8w)	(3, 4h, 4w)
Dual 2	Conv <sub>s2</sub> -LeakyReLU-Conv	(3, 4h, 4w)	(3, 2h, 2w)
Dual 3	Conv <sub>s2</sub> -LeakyReLU-Conv	(3, 2h, 2w)	(3, 1h, 1w)

## APPENDIX D

### MORE RESULTS ON DUAL REGRESSION

In this section, we first provide an additional ablation study of the dual regression scheme on other architectures. Then, we investigate the effect of the trainable dual models on the SR performance. Last, we provide more comparison visual results to show the superiority of the proposed dual regression network over existing methods.

#### D.1 Effect of Dual Regression Scheme on Other Architectures

To verify the impact of the dual regression scheme, we also conduct an ablation study of the dual network for SRResNet. “SRResNet + Dual” denotes the baseline SRResNet equipped with the dual regression scheme. From Table B, the model with the dual regression scheme consistently outperforms the baseline counterpart, which further demonstrates the effectiveness of our method.

#### D.2 Effect of the Trainable Dual Models

Our dual regression learning scheme contains several simple dual models (each dual model only consists of two convolution layers and one LeakyReLU layer [104]), which bring some extra parameters to train. The dual models can also be a fixed degradation method



TABLE B

The impact of the proposed dual regression scheme on the SRResNet model in terms of PSNR score on the five benchmark datasets for  $4\times$  SR.

Method	Set5	Set14	BSDS100	Urban100	Manga109
SRResNet	32.26	28.53	27.61	26.24	31.03
SRResNet + Dual	<b>32.47</b>	<b>28.77</b>	<b>27.70</b>	<b>26.58</b>	<b>31.24</b>

(*i.e.*, Bicubic), but a fixed degradation method may not be helpful to reduce the possible function space, resulting in a limited SR performance. To verify the necessity of the trainable dual models, we investigate the effect of the dual model whether it is trainable or not (See the results in Table C). “DRN-S with fixed dual” denotes the model using a fixed degradation method (*i.e.*, Bicubic) to form the closed-loop. From Table C, the model with trainable dual models significantly outperforms the counterpart using the fixed degradation method, which demonstrates the necessity of the trainable dual models.

TABLE C

Comparisons of the DRN-S models equipped with the trainable dual model and the fixed dual degradation method for  $4\times$  SR.

Method	Set5	Set14	BSDS100	Urban100	Manga109
DRN-S with fixed dual	32.31	28.51	27.45	26.27	31.04
DRN-S (Ours)	<b>32.68</b>	<b>28.93</b>	<b>27.78</b>	<b>26.84</b>	<b>31.52</b>

### D.3 More Comparisons and Results

For supervised super-resolution, we put more visual results in this section shown in Figures B and C, respectively. From these results, our models are able to produce the images with sharper edges and clearer textures than state-of-the-art methods.

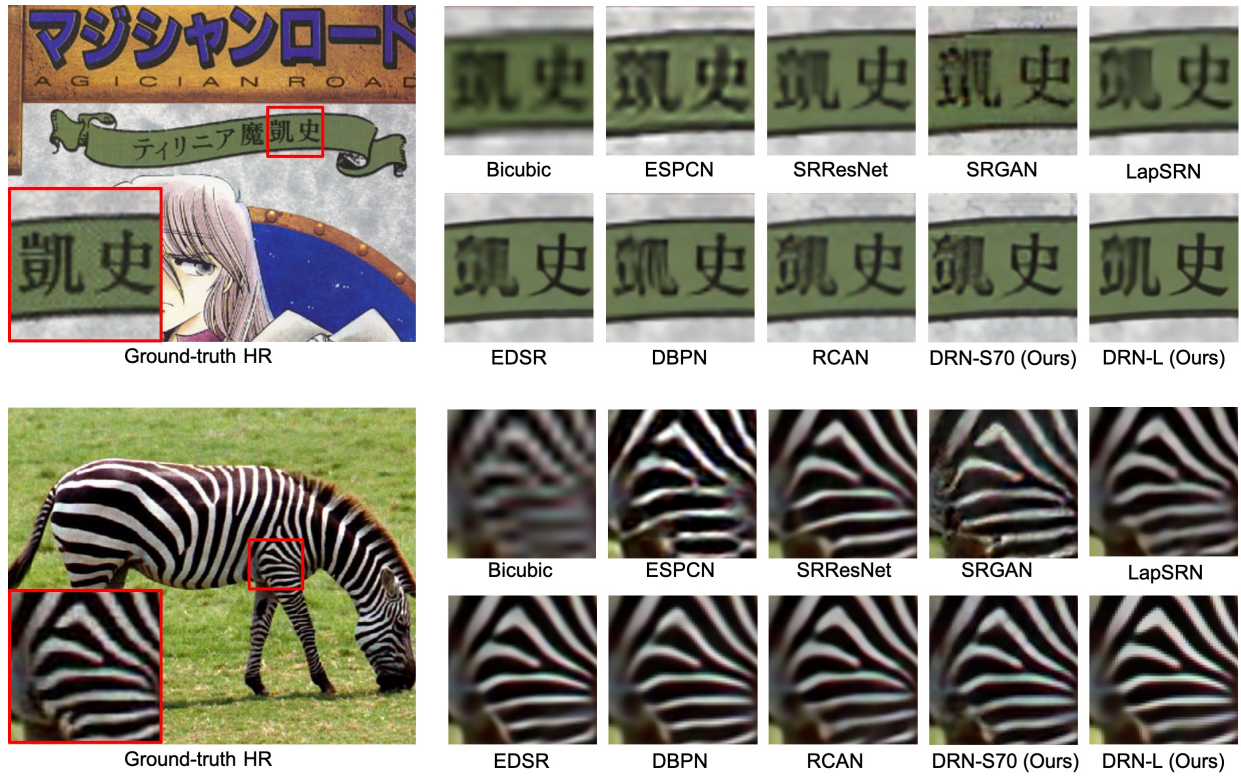


Fig. B. Visual comparison for  $4\times$  image super-resolution on benchmark datasets.

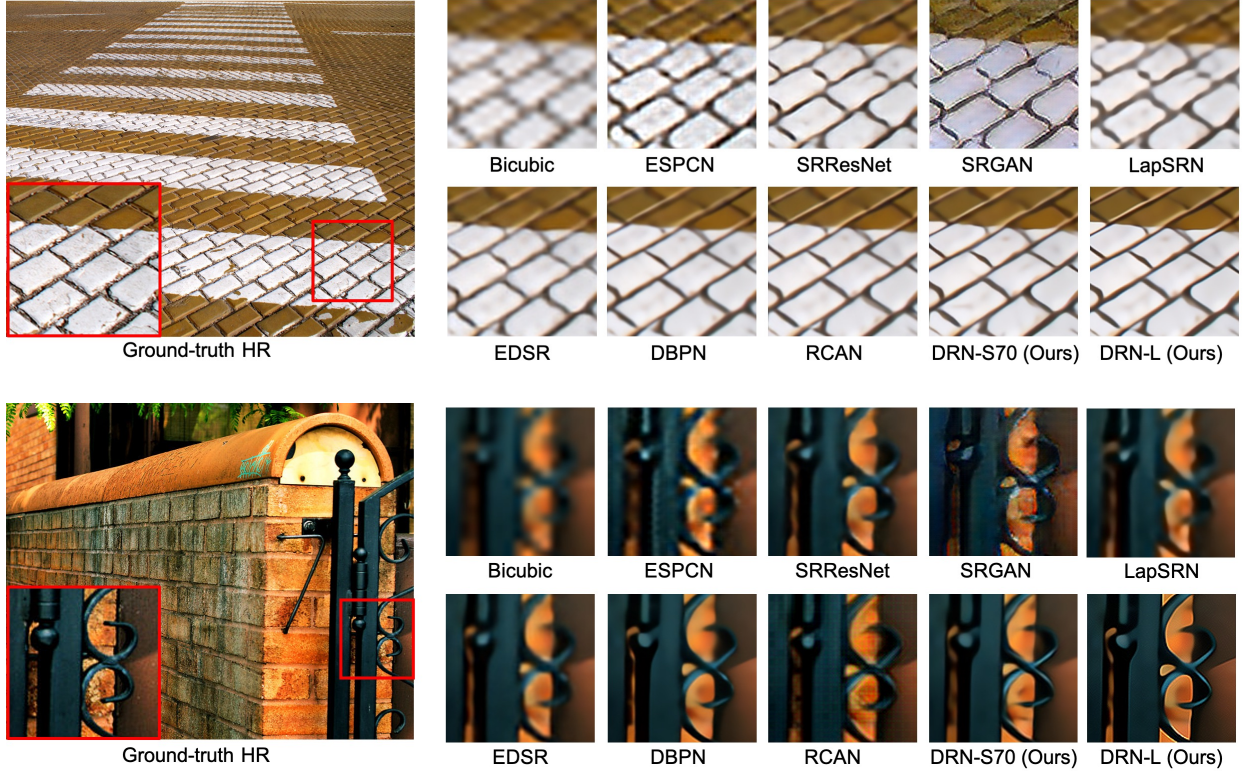


Fig. C. Visual comparison for  $8\times$  image super-resolution on benchmark datasets.

## APPENDIX E

### ADAPTATION RESULTS ON UNPAIRED DATA

In this experiment, we apply the proposed method to a variety of real-world unpaired data. Different from the supervised setting, we first consider a toy case where we evaluate SR models on the LR images with different degradation methods (*e.g.*, Nearest and BD [40]). During training, we can only access the LR images but not their corresponding HR images. Then, we also apply our method to LR raw video frames from YouTube.

#### E.1 Datasets and Implementation Details

In this experiment, we obtain the paired synthetic data by downsampling existing images. Considering the real-world SR applications, all the paired data belong to a different domain from the unpaired data. Following [2], we randomly choose 3k images from ImageNet (called ImageNet3K) and obtain LR images using different degradation methods, including Nearest and BD. We adopt DIV2K (Bicubic) as the paired synthetic data (We can also use other degradation methods to obtain the paired synthetic data. We put the impact of degradation methods in Section E.5) and ImageNet3K LR images with different degradations as the unpaired data. Note that ImageNet3K HR images are not used in our experiments. For the SR task on real-world videos, we collect 3k raw video frames as the unpaired data to train the models.

We use our DRN-S to evaluate the proposed adaptation algorithm and call the resultant models DRN-Adapt. For quantitative comparison on unpaired synthetic data, we obtain the LR images of five benchmark datasets using Nearest and BD degradation methods separately. We train a DRN-Adapt model for each kind of unpaired data, *i.e.*, Nearest data, BD data, and video frames collected from YouTube. Thus, there are 3 DRN-adapt models in total. Based on pretrained DRN-S, We train our DRN-Adapt models with a learning rate of  $10^{-4}$  and the data ratio of unpaired data  $\rho = 30\%$  for a total of  $10^5$  iterations. Moreover, we apply Adam with  $\beta_1 = 0.9$ ,  $\beta_2 = 0.99$  to optimize the models, and set minibatch size as 16. And we also train a CinCGAN [70] model for each kind of unpaired data for comparison.

#### E.2 Comparison on Unpaired Synthetic Data

To evaluate the adaptation performance on unpaired data, we compare our DRN-Adapt and the baseline methods on synthetic data. We report the PSRN and SSIM values of different methods for  $8\times$  super-resolution in Table D. From Table D, DRN-Adapt consistently outperforms the supervised methods on all the datasets. For CycleGAN based SR method, CinCGAN achieves better performance than the supervised learning methods but still cannot surpass our method due to the inherent limitations mentioned before. Note that for the Nearest LR data, we also report the recovery results of the *Nearest* kernel, which is the same as the degradation method. Our method also yields a large performance improvement over this baseline. These results demonstrate the effectiveness of the proposed adaptation algorithm on unpaired data.



Fig. D. Visual comparison of model adaptation for  $8\times$  super-resolution on real-world video frames (from YouTube).

TABLE D  
Adaptation performance of super-resolution models on images with different degradation methods for  $8\times$  SR.

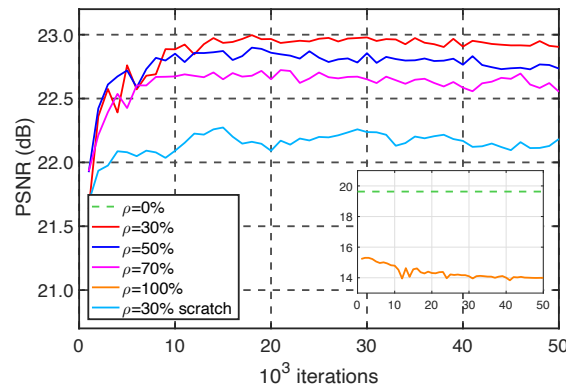
Algorithms	Degradation	Set5 PSNR / SSIM	Set14 PSNR / SSIM	BSDS100 PSNR / SSIM	Urban100 PSNR / SSIM	Manga109 PSNR / SSIM
Nearest	Nearest	21.22 / 0.560	20.11 / 0.485	20.64 / 0.471	17.76 / 0.454	18.51 / 0.594
EDSR [16]		19.56 / 0.580	18.24 / 0.498	18.53 / 0.479	15.68 / 0.435	17.22 / 0.598
DBPN [27]		18.80 / 0.541	17.36 / 0.461	17.94 / 0.456	15.07 / 0.400	16.67 / 0.550
RCAN [17]		18.33 / 0.534	17.11 / 0.436	17.67 / 0.444	14.73 / 0.380	16.25 / 0.525
CinCGAN [102]		21.76 / 0.648	20.64 / 0.552	20.89 / 0.528	18.21 / 0.505	18.86 / <b>0.638</b>
DRN-Adapt		<b>23.00 / 0.715</b>	<b>21.52 / 0.561</b>	<b>21.98 / 0.539</b>	<b>19.07 / 0.518</b>	<b>19.83 / 0.613</b>
EDSR [16]	BD	23.54 / 0.702	22.13 / 0.594	22.71 / 0.567	19.70 / 0.551	20.64 / 0.700
DBPN [27]		23.05 / 0.693	21.65 / 0.586	22.50 / 0.565	19.28 / 0.538	20.16 / 0.689
RCAN [17]		22.23 / 0.678	21.01 / 0.567	21.85 / 0.552	18.36 / 0.509	19.34 / 0.659
CinCGAN [102]		23.39 / 0.682	22.14 / 0.581	22.73 / 0.554	20.36 / 0.538	20.29 / 0.670
DRN-Adapt		<b>24.62 / 0.719</b>	<b>23.07 / 0.612</b>	<b>23.59 / 0.583</b>	<b>20.57 / 0.591</b>	<b>21.52 / 0.714</b>

### E.3 Comparison on Unpaired Real-world Data

We apply our method to YouTube raw video frames, which are more challenging owing to the complicated and unknown degradation in real-world scenarios. Since there are no ground-truth HR images, we only provide the visual comparison. From Figure D, the generated frames from three supervised baselines (*i.e.*, EDSR, DBPN, and RCAN) contain numerous mosaics. For CinCGAN, the SR results are distorted and contain a lot of noise due to the sensitivity to data differences between unpaired LR and HR images. By contrast, our DRN-Adapt produces visually promising images with sharper and clearer textures.

### E.4 Effect of $\rho$ on the Adaptation Algorithm

We investigate the effect of  $\rho$  on the proposed adaptation algorithm. We compare the performance when we change the data ratio of unpaired data  $\rho$  and show the corresponding training curves in Figure E. From Figure E, when we set  $\rho \in \{30\%, 50\%, 70\%\}$ , the resultant models obtain better performance than the baseline model, *i.e.*, with  $\rho=0\%$ . In practice, we set  $\rho=30\%$  to obtain the best performance. We also compare the models with and without the pretrained parameters. From Figure E, the model trained from scratch yields a slightly worse result but still outperforms the baseline model without adaptation. These results demonstrate the effectiveness of the proposed adaptation algorithm.

Fig. E. Comparisons of the performance on unpaired data with Nearest degradation (testing on HR with the shape of  $1280 \times 720$ ) for  $4 \times$  SR.

### E.5 Impact of Degradation Methods on Adaptation

In this experiment, we investigate the impact of different degradation methods to obtain paired synthetic data in our adaptation algorithm. We change the kernel from Bicubic to Nearest and evaluate the adaptation models on BD data. From Table E, DRN-Adapt obtain similar results when we use different degradation methods to obtain the paired synthetic data. This experiment shows that our adaptation algorithm yields relatively stable performance with different degradation methods.

TABLE E  
The impact of different degradation methods on DRN-Adapt for  $8\times$  SR.

Degradation Method	Set5	Set14	BSDS100	Urban100	Manga109
Nearest	24.60	23.03	<b>23.60</b>	<b>20.61</b>	21.46
Bicubic	<b>24.62</b>	<b>23.07</b>	23.59	20.57	<b>21.52</b>